

Abstract

Ice supersaturation in the upper troposphere is a complex and important issue for the understanding of cirrus cloud formation. Infrared sounders have the ability to provide cloud properties and atmospheric profiles of temperature and humidity. On the other hand, they suffer from coarse vertical resolution, especially in the upper troposphere and therefore are unable to detect shallow ice supersaturated layers. We have used data from the Measurements of Ozone and water vapour by Airbus in-service aircraft experiment (MOZAIC) in combination with Atmospheric InfraRed Sounder (AIRS) relative humidity measurements and cloud properties to develop a calibration method for an estimation of occurrence frequencies of ice supersaturation. This method first determines the occurrence probability of ice supersaturation, detected by MOZAIC, as a function of the relative humidity determined by AIRS. The occurrence probability function is then applied to AIRS data, independently of the MOZAIC data, to provide a global climatology of upper-tropospheric ice supersaturation occurrence. Our climatology is then related to high cloud occurrence from the Cloud-Aerosol Lidar with Orthogonal Polarization (CALIOP) and compared to ice supersaturation occurrence statistics from MOZAIC alone. Finally it is compared to model climatologies of ice supersaturation from the Integrated Forecast System (IFS) of the European Centre for Medium-Range Weather Forecasts (ECMWF) and from the European Centre Hamburg Model (ECHAM). All the comparisons show good agreements when considering the limitations of each instrument and model. This study highlights the benefits of multi-instrumental synergies for the investigation of upper tropospheric ice supersaturation.

1 Introduction

Ice supersaturation (or “ISS”, relative humidity with respect to ice larger than 100%) is a prerequisite for the nucleation of cirrus clouds (e.g. Haag et al., 2003) and for the persistence of condensation trails (Schumann, 1996). Few climate models have included

ACPD

11, 12889–12947, 2011

Ice supersaturation from the Atmospheric InfraRed Sounder

N. Lamquin et al.

Title Page

Abstract

Introduction

Conclusions

References

Tables

Figures

◀

▶

◀

▶

Back

Close

Full Screen / Esc

Printer-friendly Version

Interactive Discussion



a parametrization of supersaturation despite the growing necessity of a better representation of ice cloud formation processes (Waliser et al., 2009). While radiosounding and in situ measurements provide measurements of relative humidity at a high vertical resolution (Spichtinger et al., 2003a; Krämer et al., 2009), continuous and global observations are only achievable from satellite measurements which, in turn, suffer from a limited vertical resolution.

For example, Kahn et al. (2008) and Lamquin et al. (2008) have shown that cirrus clouds have generally a smaller vertical extent (about 2 km) than the AIRS vertical resolution (>3 km in the upper troposphere, Maddy and Barnet, 2008) and that relative humidity (RH_i) inside cirrus clouds is difficult to determine since clear parts of the profile, over or under the clouds, are taken into account in its computation. In addition, the radiances used for the retrieval of atmospheric temperature and water vapour profiles are cloud cleared (Chahine et al., 2006) and therefore these RH_i profiles correspond more to the atmosphere around the clouds. Thus RH_i distributions in the presence of cirrus clouds show dry biases when compared to in situ measurements and model parametrizations (e.g. Lamquin et al., 2009).

Ice supersaturation (RH_i $> 100\%$) occurs over even thinner portions of the atmosphere (about 500 m according to Spichtinger et al., 2003a), it is thus even harder to detect by satellites (e.g. Gierens et al., 2004). As a consequence, its global frequency of occurrence is underestimated if a threshold of 100% is used (Gettelman et al., 2006a). Therefore, Stubenrauch and Schumann (2005) have taken the coarse vertical resolution of TOVS data into account by adjusting the threshold to 70%.

We now propose a more sophisticated method based on the construction of an a priori knowledge of the occurrence probability of ice supersaturation inside a vertical pressure layer as a function of the AIRS relative humidity (from now onwards termed “RH_{iA}”) computed over this vertical pressure layer.

Section 2 presents AIRS and MOZAIC datasets. Section 3 presents relationships inferred from the collocation of AIRS and MOZAIC as well as the calibration method. This method is then employed in Sect. 4, independently of the MOZAIC data, to build

Ice supersaturation from the Atmospheric InfraRed Sounder

N. Lamquin et al.

Title Page

Abstract

Introduction

Conclusions

References

Tables

Figures

◀

▶

◀

▶

Back

Close

Full Screen / Esc

Printer-friendly Version

Interactive Discussion



a climatology of ice supersaturation from the AIRS data only. Our climatology is first related to high cloud statistics from CALIOP and is evaluated with the ice supersaturation climatology determined with MOZAIC data over regions of air traffic. Then we compare it to model climatologies from ECMWF and ECHAM4. Data other than AIRS and MOZAIC are shortly introduced before each comparison in Sect. 4 because the relevance of the extracted parameters then appears in a more comprehensible manner.

2 Data handling

2.1 AIRS data, quality and vertical resolution

On board the NASA Aqua satellite, AIRS provides very high resolution measurements of Earth emitted radiation in three spectral bands from 3.74 to 15.40 μm , using 2378 channels. Observations exist at 01:30 and 13:30 local time since May 2002. The spatial resolution of these measurements is 13.5 km at nadir. Nine AIRS measurements (3×3) correspond to one footprint of the Advanced Microwave Sounder Unit (AMSU) within which atmospheric profiles of temperature T and specific humidity q are retrieved from cloud-cleared AIRS radiances at a spatial resolution of about 40 km at nadir (Chahine et al., 2006). AIRS level 2 (L2) standard products include temperature at 28 pressure levels from 0.1 hPa to the surface and water vapour mixing ratios w within 14 pressure layers from 50 hPa to the surface (Susskind et al., 2003, 2006). We investigate ISS occurrence within the 6 standard pressure layers 100–150, 150–200, 200–250, 250–300, 300–400, and 400–500 hPa. These layers are about 2 km thick.

Version 5 of AIRS L2 data provide quality flags for each atmospheric profile (Susskind et al., 2006; Tobin et al., 2006). We derive relative humidity “RH_{iA}” as in Lamquin et al. (2009) from profiles of best and good quality using the conditions Qual_{H2O} \neq 2 and PGood > 600 hPa. These correspond to about 70% of all situations.

Ice supersaturation from the Atmospheric InfraRed Sounder

N. Lamquin et al.

Title Page

Abstract

Introduction

Conclusions

References

Tables

Figures



Back

Close

Full Screen / Esc

Printer-friendly Version

Interactive Discussion



Ice supersaturation from the Atmospheric InfraRed Sounder

N. Lamquin et al.

Title Page

Abstract

Introduction

Conclusions

References

Tables

Figures

◀

▶

◀

▶

Back

Close

Full Screen / Esc

Printer-friendly Version

Interactive Discussion



Humidity measurements for which the water vapour content is lower than 10–20 ppmv are below the nominal instrument sensitivity and are subject to a higher uncertainty (Gettelman et al., 2004). By comparing AIRS and Microwave Limb Sounder (MLS) products Fetzer et al. (2008) show that AIRS moisture data at altitudes higher than 200 hPa may lead to misleading results. As a consequence, RH_{iA} may not be fully exploitable at pressure levels higher than 200 hPa. However, Montoux et al. (2009) suggest that these data can be used even though they are less precise. We decide to include these data as the results at such altitudes (pressure layers 100–150 an 150–200 hPa) are indicative. Nevertheless, caution warnings recall the reader's attention throughout the analysis.

We also use cloud properties retrieved at LMD (Stubenrauch et al., 2010) for each AIRS footprint at the spatial scale of about 13.5 km. This global cloud climatology, covering the period from 2003 to 2008, provides cloud pressure p_{clid} and emissivity ϵ_{clid} thus allowing a distinction between clear skies, low, middle, and high cloudiness. In addition, high clouds are further distinguished according to cloud emissivity, as high opaque clouds ($\epsilon_{\text{clid}} > 0.95$), cirrus ($0.95 > \epsilon_{\text{clid}} > 0.5$) and thin cirrus ($0.5 > \epsilon_{\text{clid}}$). Their global coverage is about 2%, 11% and 9%, respectively. However, considering only situations with atmospheric profiles retrieved with good quality, their fractions change to about 0%, 5% and 10%, respectively. Combining all seasons, Table 1 shows these statistics (for high clouds and for other situations) separately for good quality data and for any data. The statistics are made globally, for tropics only and for northern mid-latitudes only. Therefore, high clouds for which AIRS provides atmospheric profiles of good quality consist of all thin cirrus and of half of the cirrus category. In the following, we use the general term “cirrus”, including both categories, with exception of Sect. 3.4, where we distinguish between both categories.

2.2 MOZAIC data

The MOZAIC experiment (Marenco et al., 1998) gathered concentrations of ozone and water vapour mainly in the upper troposphere/lower stratosphere (UTLS) region from

measurements aboard commercial airplanes over the period August 1994–December 2007. The accuracy of the water vapour measurements is an asset for locally detecting ice supersaturation in the UTLs (Gierens et al., 1999).

However, this database only covers the main flight routes of European airliners involved in the project (Marenco et al., 1998), and it is impossible to obtain a global coverage. In addition, the small amount of aircraft equipped with probing sondes as well as the randomness and the seasonal variability of flight destinations induce a non-uniform spatial and temporal representation.

Figure 1 highlights this fact for upper tropospheric data ($p_M < 500$ hPa, where p_M stands for the flight altitude) over the period 2002–2007. The top figure shows the fraction of measurements, in a $5^\circ \times 5^\circ$ grid, taken in summer compared to the statistics including winter and summer for each latitude/longitude. The very large variability indicates that these data will sometimes include more statistics from winter measurements (over the Arctic for example) or from summer measurements (over Russia for example).

Moreover, statistics in each grid box are not sampled within regular time steps. To illustrate this, the bottom figure of Fig. 1 shows the average interval (in days) between overpasses for each grid box. Except on very common routes, such as the North-Atlantic Flight Corridor, overpasses are not obtained on a daily basis. Rather, about 5 days are necessary for further overpasses of a region, which is very sparse for accurate statistics. 352 grid boxes have an average time step smaller than 10 days but 273 grid boxes have an average time step larger than 10 days, 67 grid boxes attain average delays larger than 100 days.

We derive relative humidity with respect to ice “RH_{iM}” as in Gierens et al. (1999) and only keep data of highest quality (tag “1”) with $p_M < 500$ hPa and $T < 243$ K so that we avoid mixed-phase relative humidities (e.g. Pruppacher, 1994). Moreover, the same procedure as in Gierens et al. (1999) is applied to find out if measurements were taken in the lower stratosphere or in the upper troposphere. An ozone mixing ratio m_{O_3} of 130 ppbv is used as a threshold separating troposphere (lower values) and

Ice supersaturation from the Atmospheric InfraRed Sounder

N. Lamquin et al.

Title Page

Abstract

Introduction

Conclusions

References

Tables

Figures

◀

▶

◀

▶

Back

Close

Full Screen / Esc

Printer-friendly Version

Interactive Discussion



stratosphere (higher values). We have collocated these data with the AIRS data to (1) investigate relationships between MOZAIC relative humidity and AIRS cloud properties and (2) to develop a calibration method for the detection of ice supersaturation within the AIRS data.

3 Synergy of AIRS and MOZAIC

3.1 AIRS-MOZAIC collocations and statistics

AIRS cloud properties are retrieved within each AIRS footprint of 13.5 km whereas RH_{iA} is computed within the AMSU footprint of about 40 km. Therefore, we use two different collocation schemes. When combining the AIRS cloud properties with MOZAIC RH_i measurements we only keep the one flight measurement which is closest to the center of the AIRS footprint and which is inside the AIRS footprint. When combining the AIRS relative humidity RH_{iA} with MOZAIC RH_i we first collect all MOZAIC single measurements located within the AMSU footprint and then choose the highest relative humidity RH_{iM} among the collection of collocated measurements. In both cases data have to be coincident within a timeframe of 30 min.

The situation is illustrated in Fig. 2 where a MOZAIC flight is crossing an AMSU footprint. A maximum of about 50 collocated MOZAIC measurements (from one flight) can reside within one AMSU footprint. The high coverage and the large amount of AIRS data between 2003 and 2007 lead to a relatively large set of statistics. Table 2 shows statistics of collocated events (one MOZAIC single measurement per AIRS footprint) in the upper troposphere ($p < 500$ hPa) per latitude band and per AIRS scene divided into clear sky (“clear”), low and mid-level clouds (“lmclds”, $p_{\text{cld}} > 440$ hPa) and high clouds (“cirrus”, $p_{\text{cld}} < 440$ hPa). In brackets we indicate the fraction of all MOZAIC-AIRS collocations with respect to the total number of events per latitude band and with respect to the total number of collocations. A large majority of the collocations are located outside of the tropical band, linked to the density of commercial flights.

Ice supersaturation from the Atmospheric InfraRed Sounder

N. Lamquin et al.

Title Page

Abstract

Introduction

Conclusions

References

Tables

Figures

⏪

⏩

◀

▶

Back

Close

Full Screen / Esc

Printer-friendly Version

Interactive Discussion



In the presence of cirrus clouds, keeping MOZAIC measurements close to the cirrus altitude ($|\rho_M - \rho_{\text{cld}}| < 50$ hPa because of the cloud top uncertainty of AIRS) leads to a considerable reduction of the global cirrus statistics: 30% of the statistics are kept. The fraction of the total number of collocations representing measurements inside cirrus then decreases from 25% to about 8%. This is in agreement with Spichtinger et al. (2004) who find between 2 and 8% at latitudes higher than 30° and between 13 and 33% at latitudes lower than 30° based on fits of the distributions of relative humidity from the MOZAIC data.

3.2 Relationships between MOZAIC relative humidity and AIRS-LMD cloud properties

Figure 3 shows distributions of RH_{M} , separately for three scene types: cirrus, clear sky and clouds with cloud-top pressure larger than 440 hPa (low and mid-level clouds). We compare two latitude bands: northern midlatitudes $40\text{--}60^\circ$ (left) and tropics $20^\circ\text{N--}20^\circ\text{S}$ (right). For clear and Imclds situations RH_{M} corresponds to measurements within the 200–250 and 250–300 hPa layers. In the case of cirrus, RH_{M} is measured close to the cloud pressure with $|\rho_M - \rho_{\text{cld}}| < 50$ hPa so that the distributions begin to represent what might actually be observed inside a cirrus layer. For every situation data are only considered below the tropopause. This is ensured by the MOZAIC criterion $m_{\text{O}_3} < 130$ ppbv and by the tropopause altitude provided in the AIRS L2 data.

In both latitude bands the distributions for clear skies are similar to those for low and middle clouds. We observe drier upper tropospheric air in the tropics at aircraft cruise altitudes (mainly about 200–250 hPa), consistent with Fig. 4 of Gierens et al. (1999). For situations involving cirrus clouds we observe a peak frequency at 115–120% for the northern midlatitudes and around 100% for the tropics. In the tropics, the cruise altitude of aircraft does not coincide with the altitude where cirrus clouds are most commonly found (100–150 hPa in Lamquin et al., 2008). Therefore it is likely that relatively drier values and a larger standard deviation in this region are induced by the presence of dissipating cirrus and, possibly, shallower ice supersaturated layers.

Ice supersaturation from the Atmospheric InfraRed Sounder

N. Lamquin et al.

Title Page

Abstract

Introduction

Conclusions

References

Tables

Figures

◀

▶

◀

▶

Back

Close

Full Screen / Esc

Printer-friendly Version

Interactive Discussion



**Ice supersaturation
from the Atmospheric
InfraRed Sounder**

N. Lamquin et al.

Title Page

Abstract

Introduction

Conclusions

References

Tables

Figures

◀

▶

◀

▶

Back

Close

Full Screen / Esc

Printer-friendly Version

Interactive Discussion



The peak value for the northern midlatitudes is wetter than expected from in situ measurements (Ovarlez et al., 2002; Immler et al., 2008). In fact, these authors show distributions of relative humidity inside cirrus clouds peaked around saturation. Our observation of a peak higher than saturation agrees with the distributions of RH_{iM} (measured in 2003) in Gettelman et al. (2006a) where RH_{iM} decreases more sharply after 120% but disagrees with distributions from Gierens et al. (1999) obtained from earlier MOZAIC data (1995–1997). Indeed, Gierens et al. (1999) show probability distributions of either tropospheric or stratospheric RH_{iM} . These distributions show a decrease beyond 100% with a concomitant bulge highlighting the statistics of measurements inside cirrus clouds (Spichtinger et al., 2004). Figure 4 compares distributions of tropospheric RH_{iM} ($p < 500$ hPa, $T < 243$ K and $m_{\text{O}_3} < 130$ ppbv) obtained from MOZAIC-only data between 1995 and 1997 to distributions obtained from data between 2002 and 2004 and between 2005 and 2007. Compared to the years 1995 to 1997 the distributions over the periods 2002–2004 and 2005–2007 show a strong bias of about 10%, likely due to a calibration problem.

In the following we consider the occurrence of ice supersaturation detected by MOZAIC. For this purpose we need to take the measurement bias (for the MOZAIC time period used here: 2002–2007) into account by shifting the detection threshold by 10%: MOZAIC detects ice supersaturation only when $\text{RH}_{iM} > 110\%$. This is all the more reliable since the shape of the decreasing slope after saturation is unchanged. Also, as Gierens et al. (1999) suggest for values of RH_{iM} around saturation, an uncertainty $\Delta\text{RH}_{iM} = \pm 10\%$ is taken into account.

3.3 Impact of fixed flight altitudes

We have to keep in mind that MOZAIC measurements are taken at only one level, corresponding to the actual flight altitude. There is no information on the thickness of supersaturated layers. Even if the MOZAIC measurement is below an assumed ISS threshold of 110%, there may exist a layer of ISS below or above flight altitude. This potentially underestimates the occurrence of ice supersaturation detected by MOZAIC within the AIRS pressure layers of about 2 km.

To compensate for this effect we must lower the relative humidity threshold for ice supersaturation detection in MOZAIC. On the other hand, lowering this threshold increases the probability of false-alarms, that is to say the amount of supersaturation detected when there is no supersaturation in reality.

5 A new threshold has therefore been determined by simulating the success to detect supersaturation in a collection of radiosoundings from routine measurements at Lindenberg, Germany. These radiosounding measurements are corrected in the upper troposphere (Leiterer et al., 2005) and detect ice supersaturation (Spichtinger et al., 2003a; Lamquin et al., 2009).

10 The principle is the one of the Peirce skill-score (Peirce, 1884). It has notably been used (and widely explained) in Rädcl and Shine (2007) for an evaluation of the ability of radiosounding measurements to detect cold ice supersaturated regions nesting persistent contrails.

15 For each AIRS pressure layer with top pressure larger than or equal to 200 hPa (because of the altitude of the tropopause in Lindenberg) a Monte-Carlo simulation is made over the collection of radiosonde profiles: it simulates for each profile a random altitude and, thus, a random measurement of relative humidity inside a pressure layer. An evaluation of the success to detect ice supersaturation by applying a threshold of relative humidity lower than saturation is made using the Peirce skill-score. It is simulated for each relative humidity threshold between 0 and 100%.

20 Figure 5 shows the skill-scores obtained for each of the four AIRS pressure layers between 200 and 500 hPa. For the pressure layers 200–250 and 250–300 hPa the score is maximum for a relative humidity threshold of about 90%. The distributions for the pressure layers 300–400 and 400–500 hPa are slightly broader with a peak around 85%. The difference is linked to the slightly larger vertical extension of these layers.

25 In the AIRS-MOZAIC collocations most of the statistics arise from flight altitudes between 200 and 300 hPa, therefore the skill-scores obtained for the pressure layers 200–250 and 250–300 hPa in Fig. 5 must preferably be taken into account. As a consequence, a decrease of 10% is applied to the MOZAIC relative humidity threshold for

Ice supersaturation from the Atmospheric InfraRed Sounder

N. Lamquin et al.

[Title Page](#)[Abstract](#)[Introduction](#)[Conclusions](#)[References](#)[Tables](#)[Figures](#)[⏪](#)[⏩](#)[◀](#)[▶](#)[Back](#)[Close](#)[Full Screen / Esc](#)[Printer-friendly Version](#)[Interactive Discussion](#)

the detection of ice supersaturation within the boundaries of the AIRS pressure layers. To conclude, we consider ISS to be detected by MOZAIC at some location of a pressure layer when $RH_{iM} > 100 \pm 10\%$. Although this threshold would have naturally been used, only an understanding of the relationships presented above leads to its correct interpretation.

3.4 A calibration method for the determination of ice supersaturation occurrence within AIRS pressure layers

The principle of the method was introduced in Lamquin et al. (2009). It is based on the determination of an occurrence probability of ISS as a function of coarse relative humidity measurements integrated over pressure layers. This occurrence probability can either be the probability of “at least once” supersaturation (supersaturation exists somewhere within the layer) or the probability of supersaturation weighted by the thickness of the supersaturated fraction of the layer (the weight being one if supersaturation covers the whole pressure layer). The first approach is equivalent to the second approach when using a weight of one, whether the supersaturated layer is thin or thick. According to Spichtinger et al. (2003a) and Rädcl and Shine (2007) ice supersaturated layers are indeed on average thinner (about 500–700 m) than the vertical spacing of the AIRS pressure layers (about 2 km). In Lamquin et al. (2009) the “at least once” approach was proposed because no accurate information on the thickness of supersaturated layers could be given. Dickson et al. (2010) investigated the weighted approach by using a very large set of radiosonde measurements, they show that the so-called “S-function” depends mostly on the vertical resolution of the coarsely-determined relative humidity.

As MOZAIC measurements do not allow the determination of the thickness of ice supersaturated layers, we must use the “at least once” approach and make a sensitivity analysis. The “at least once” statistics lead to higher ISS occurrences than the statistics weighted by the thickness of the supersaturated layers (Figs. 3 and 4 of Rädcl and Shine, 2007). This is important to keep in mind when comparisons are presented in Sect. 5 as we will compute ISS occurrence frequencies in other datasets in a similar way over pressure layers of finite depth.

Ice supersaturation from the Atmospheric InfraRed Sounder

N. Lamquin et al.

Title Page

Abstract

Introduction

Conclusions

References

Tables

Figures

◀

▶

◀

▶

Back

Close

Full Screen / Esc

Printer-friendly Version

Interactive Discussion



Ice supersaturation from the Atmospheric InfraRed Sounder

N. Lamquin et al.

Title Page

Abstract

Introduction

Conclusions

References

Tables

Figures

◀

▶

◀

▶

Back

Close

Full Screen / Esc

Printer-friendly Version

Interactive Discussion



We now build the “S-function” by examining the probability of ice supersaturation computed from MOZAIC data collocated with AIRS relative humidity RH_{iA} . We reject AIRS bad quality data as well as RH_{iA} computed in pressure layers inside of which a tropopause is observed. Figure 6 then relates RH_{iA} and $S_{Th}(RH_{iA})$, the occurrence probability of ice supersaturation determined by the condition $RH_{iM} > Th\%$ with either $Th = 90\%$, $Th = 100\%$ or $Th = 110\%$ to take into account the 10% uncertainty of MOZAIC.

The statistics drop progressively as RH_{iA} increases, without enough statistics at $RH_{iA} > 100\%$ (less than 100 events per interval). Only statistically significant pairs (RH_{iA} , $S_{Th}(RH_{iA})$) are shown, and each curve is fitted with a hyperbolic tangent for further use.

Two conclusions can be drawn: first, we see that, even for $Th = 110\%$, a significant probability of ice supersaturation is found when RH_{iA} is smaller than 100%. This is what we expected, as Kahn et al. (2008) and Lamquin et al. (2008) have already shown that very shallow ice clouds are concomitant with low RH_{iA} , highlighting the impact of the coarse vertical resolution of the sounder.

Second, the occurrence of ice supersaturation reaches only about 85% for RH_{iA} values around saturation even for $Th = 90\%$. It can be argued that MOZAIC does not always locate ISS lying within the pressure layer even though we statistically compensate the effect of having fixed flight altitudes in the timeframe of the collocation. However, when $RH_{iA} \approx 100\%$ a substantial part of the pressure layer must be very humid thus decreasing the probability that MOZAIC misses ISS. Another explanation considers non-linear effects of the AIRS vertical resolution on RH_{iA} . Unfortunately it is not possible to investigate it further as we do not have information on relative humidity profiles with MOZAIC.

To explore the stability of the S-function Fig. 7 distinguishes latitude bands (top left), seasons in the northern midlatitudes (top right), cloud scenes as inferred from the nine AIRS footprints within each AMSU footprint (bottom left) and temperature intervals given by the MOZAIC measurements (bottom right). Only RH_{iA} values lower than

saturation are shown because higher values do not provide enough statistics. In Fig. 7 occurrence probabilities of ice supersaturation are determined with $T_h = 100\%$. The regional and seasonal variabilities are rather small compared to variabilities obtained for different temperature ranges or cloud scenes.

5 The interpretation of the differences observed for different cloud scenes is quite straightforward. We distinguish between clear and cloudy situations in the upper troposphere: “clear” meaning “no clouds in the upper troposphere”, that is to say either clear sky or low and mid-level clouds. Using the retrieved emissivity we further separate cirrus situations into “thin cirrus” ($\epsilon_{\text{cld}} < 0.5$) and “cirrus” ($\epsilon_{\text{cld}} > 0.5$). Clearly, the occurrence probability of ice supersaturation $S(\text{RH}_{iA})$ is increasing with cloudiness in the upper troposphere. This highlights the effect of fixed flight altitudes of MOZAIC within the AIRS pressure layers. With increasing cloudiness portions of the atmospheric profiles with high relative humidity are extending vertically, thus increasing the probability for MOZAIC aircraft to fly through supersaturated areas (either inside or in the vicinity of clouds). On average, the impact of fixed flight altitudes has been taken into account by lowering the MOZAIC detection threshold T_h . It could be considered relevant to use different S-functions depending on the cloud scene but we are interested in the occurrence of ice supersaturation within a pressure layer, independently of its vertical extent. The differences in Fig. 7 for different cloud scenes should not be considered as a bias in the present analysis.

15 For different temperature ranges there is no clear distinction between results obtained for the temperature ranges $220 < T < 230 \text{ K}$ and $T > 230 \text{ K}$ (with still $T < 243 \text{ K}$). However, Fig. 7 exhibits higher occurrence probability of ice supersaturation for the coldest temperatures ($T < 220 \text{ K}$). Gierens et al. (1999) show that ice supersaturated regions are, on average, colder than other regions in the upper troposphere. By selecting the coldest temperatures we might in turn get higher ice supersaturation occurrence probability simply by having a greater chance that MOZAIC meets supersaturation. Possible non-linear effects of the AIRS vertical resolution on RH_{iA} might influence this comparison as temperature can vary as much as 5 to 10 K between the edges of the

Ice supersaturation from the Atmospheric InfraRed Sounder

N. Lamquin et al.

[Title Page](#)[Abstract](#)[Introduction](#)[Conclusions](#)[References](#)[Tables](#)[Figures](#)[⏪](#)[⏩](#)[◀](#)[▶](#)[Back](#)[Close](#)[Full Screen / Esc](#)[Printer-friendly Version](#)[Interactive Discussion](#)

pressure layers and MOZAIC can fly anywhere inside the layer. We can therefore only relate the observed differences to global uncertainties. Again, we cannot investigate this any further as MOZAIC does not provide information on the vertical distribution of temperature and humidity.

5 Overall the S-function appears quite stable with differences remaining within the uncertainties arising from MOZAIC and its coupling with AIRS. The global uncertainty on this method is set by the two bracketing S-functions $S_{90}(\text{RH}_{iA})$ and $S_{110}(\text{RH}_{iA})$.

3.5 Horizontal extent of ice supersaturated areas

10 The horizontal extent of ice supersaturated layers is a key feature for a large-scale model's parameterization of ice supersaturation. Ice supersaturation can be detected from each AIRS observation only in a probabilistic way. In fact the S-function only gives the probability $S(\text{RH}_{iA})$ that an observation contains ice supersaturation. To evaluate the horizontal extent of ice supersaturated areas, we link neighbouring observations satisfying the same condition on this probability: $S(\text{RH}_{iA}) > \alpha$. To do so we built a simple clustering algorithm which groups AIRS observations belonging to the same orbits and satisfying such condition with either $\alpha = 40\%$, $\alpha = 60\%$, or $\alpha = 80\%$. Each observation is assigned the size of a square, the side of which is the diameter of the AMSU footprint and we take into account the variability of this size with the angle of observation. Clusters are constructed by grouping neighbouring observations of the same orbits and we do not relate adjacent orbits, therefore the clusters are limited by the size of the AIRS swath (1650 km). The results possibly underestimate the true size of the clusters but the figures suggest that only very few clusters are extremely large.

15 Figure 8 shows the distributions of the characteristic size (square root of the total area) of the clusters for (left) the three values of α for all regions combined and for (right) $\alpha = 80\%$ for three latitude bands: polar, ($> 70^\circ$), midlatitudes (40° – 60° N and S) and tropics (20° N– 20° S). When α is smaller the condition $S(\text{RH}_{iA}) > \alpha$ is less restrictive and therefore the cluster sizes get larger. At fixed $\alpha = 80\%$ the cluster sizes are larger in the polar regions and in the tropics, concomitant with higher ISS occurrence

Ice supersaturation from the Atmospheric InfraRed Sounder

N. Lamquin et al.

Title Page

Abstract

Introduction

Conclusions

References

Tables

Figures

◀

▶

◀

▶

Back

Close

Full Screen / Esc

Printer-friendly Version

Interactive Discussion



frequencies, than in the midlatitudes (see below Fig. 10). Overall, the large majority of characteristic sizes are smaller than 200 km which agrees qualitatively with Gierens and Spichtinger (2000).

These distributions can be fitted by Weibull distributions (Gierens and Brinkop, 2002), i.e. functions of the form $abx^{b-1}e^{-ax^b}$. Using their cumulative distribution $F(x) = 1 - e^{-ax^b}$ a linear relationship exists between $\log\log 1/(1-F)$ and $\log(x)$ as $\log\log 1/(1-F) = \log(a) + \log\log(e) + b\log(x)$ (\log is here with base 10). The histograms in Fig. 8 are then easily fitted using this relationship and Table 3 shows the parameters a and b of the Weibull function associated with each of these histograms as well as the very good correlation coefficient between the fit and the original histogram.

4 Climatology of the occurrence of ice supersaturation from AIRS

4.1 Climatology of ice supersaturation from AIRS

We have built a climatology of ice supersaturation occurrence by using $S_{100}(\text{RH}_{iA})$ as a weighting function over each value RH_{iA} determined from the AIRS observations. The uncertainties are estimated by using $S_{90}(\text{RH}_{iA})$ and $S_{110}(\text{RH}_{iA})$. To avoid potential mixed-phase situations we include a temperature condition \mathcal{T} which is either 0 or 1. \mathcal{T} is set to zero when the temperature at the bottom of the pressure layer is higher than 243 K.

ISS occurrence frequencies are computed at a spatial resolution of $1^\circ \text{ lat} \times 1^\circ \text{ lon}$ for each pressure layer p as

$$\text{ISS}_p = \frac{\sum_{i=1}^N S_{100}(\text{RH}_{iA}) \times \mathcal{T}}{N} \quad (1)$$

where N is the number of profiles of good quality in the upper troposphere over $1^\circ \times 1^\circ$. To estimate the effect of a possible bias arising from this selection, Fig. 9 presents

Ice supersaturation from the Atmospheric InfraRed Sounder

N. Lamquin et al.

Title Page

Abstract

Introduction

Conclusions

References

Tables

Figures

◀

▶

◀

▶

Back

Close

Full Screen / Esc

Printer-friendly Version

Interactive Discussion



the distributions of MOZAIC relative humidities RH_{iM} when these measurements are collocated with either good quality AIRS data or all AIRS data. The slightly wetter distribution obtained for all situations indicates that ice supersaturation occurrence ISS_p may be slightly underestimated when only good quality AIRS profiles are used.

Figure 10 presents our 6-yr (2003–2008) climatology of ice supersaturation occurrence in the upper troposphere for six AIRS pressure layers between 100 and 500 hPa. We have averaged daytime and nighttime observations. We recall that results for pressure layers 100–150 and 150–200 hPa are only indicative because of the AIRS lower reliability at such high altitudes.

Whereas the function $S(RH_{iA})$ is obtained from tropospheric data only, it is also used when the pressure layer is partly or entirely within the stratosphere. In these cases RH_{iA} is an “average” between the moister part of the layer lying in the troposphere and the drier part lying in the stratosphere. RH_{iA} is decreased compared to its tropospheric counterpart. However, $S(RH_{iA})$ is also decreased which represents the fact that ice supersaturation occurrence probability within the entire pressure layer is decreased. We assume that the S-function $S(RH_{iA})$ smoothly captures the transition from tropospheric to stratospheric air and ISS_p decreases accordingly as we progress upward.

In Fig. 10 ice supersaturation occurrence frequencies mainly follow the tropopause with high frequencies close to the tropical tropopause in the pressure layer 100–150 hPa, local maxima in connection with the storm tracks and jet streams in the mid-latitudes at 200–250 hPa, and then close to the Arctic tropopause (about 300 hPa). Although only indicative, the tropical maximum at 100–150 hPa agrees qualitatively with clear-sky ISS statistics from the Microwave Limb Sounder (MLS) in Spichtinger et al. (2003b) at 147 hPa with frequencies up to 50% over areas of deep convection. The seasonal difference between winter and summer is presented in Fig. 11. It shows higher supersaturation frequencies during boreal winter, which again agrees with Spichtinger et al. (2003b). It is induced by a stronger convection over this period.

In the polar regions Treffeisen et al. (2007) show occurrence frequencies of ISS from 15 yr of corrected radiosonde measurements over Ny-Ålesund, Svalbard. They show a

Ice supersaturation from the Atmospheric InfraRed Sounder

N. Lamquin et al.

Title Page

Abstract

Introduction

Conclusions

References

Tables

Figures



Back

Close

Full Screen / Esc

Printer-friendly Version

Interactive Discussion



strong seasonal cycle of ISS frequencies with a maximum during boreal winter (about 35% in some portions of the atmosphere in their Fig. 6), in agreement with our results.

Figure 12 shows the zonal means of ISS occurrences for winter (black lines) and summer (red lines) separately using $S_{100}(\text{RH}_{iA})$ (plain) and the uncertainties $S_{90}(\text{RH}_{iA})$ and $S_{110}(\text{RH}_{iA})$ (dashed). As can be deduced from Fig. 6, the uncertainty is about $\pm 20\%$ of the frequency values (i.e. lower for smaller ISS occurrence frequencies). The highest ISS occurrence frequencies are found close to the tropopause in the tropics and in the polar regions with maxima of about 50%.

4.2 Evaluation with MOZAIC

Although the climatology from MOZAIC is not global, an evaluation of the AIRS climatology can be made over areas covered by the MOZAIC flight paths (northern mid-latitudes mainly). We restrict the analysis to the period 2002–2007 common to both datasets.

To compute ISS occurrence with MOZAIC we follow Gierens et al. (2000) and collect MOZAIC data over $5^\circ \text{ lat} \times 5^\circ \text{ lon}$ grid cells, separately in the three pressure layers 150–200, 200–250 and 250–300 hPa. For these layers the MOZAIC statistics are the most plentiful. Only grid cells with statistics of more than one hundred measurements are kept. Both tropospheric and stratospheric data are used. We remind that ice supersaturation occurrence from AIRS represents the occurrence of supersaturation at any altitude within a pressure layer (“at least once” supersaturation occurrence). Therefore, it is important to determine ISS occurrence frequencies for MOZAIC in a similar manner. We use the same relative humidity threshold for the detection of ice supersaturation in the MOZAIC data as the one used to construct the S-function, that is to say $\text{RH}_{iM} > 100\%$. We have lowered the relative humidity threshold to compensate for the fact that MOZAIC does not detect supersaturation at altitudes below or above flight altitude and between the pressure layer boundaries (see Sect. 3.3). The ISS frequencies from MOZAIC are then slightly higher in our calculation than the one in Gierens et al. (2000). As Fig. 4 supports, it can be shown that the statistics using $\text{RH}_{iM} > 110\%$

Ice supersaturation from the Atmospheric InfraRed Sounder

N. Lamquin et al.

Title Page

Abstract

Introduction

Conclusions

References

Tables

Figures

◀

▶

◀

▶

Back

Close

Full Screen / Esc

Printer-friendly Version

Interactive Discussion



over the period 2002–2007 are comparable to the statistics using $RH_{iM} > 100\%$ over the period 1995–1997.

Figure 13 presents maps of ISS occurrences from AIRS (left) and MOZAIC (right) for the years 2002–2007 and separately for the pressure layers 150–200, 200–250, and 250–300 hPa. For an easier comparison we mask the AIRS data corresponding to grid cells where MOZAIC data are available. Geographical patterns and magnitudes agree fairly well considering the limitations of spatial and temporal sampling by MOZAIC (Fig. 1 and Sect. 2.2). The differences are particularly apparent close to the tropopause and in regions with high seasonal variability (the Arctic for example) and/or small MOZAIC coverage. The AIRS climatology is less noisy than MOZAIC because all seasons are equally well represented.

This comparison highlights the benefit of our method exploiting the synergy between AIRS and MOZAIC. We keep the best from these two datasets: the ability to detect thin supersaturated layers from MOZAIC and the global coverage from AIRS.

4.3 Relationship with cirrus cloud occurrences from CALIOP

CALIOP (Winker et al., 2003) is the first spaceborne lidar set for a long duration mission. Its ability to determine accurate vertical profiles of clouds has been shown in the literature since its launch in 2006 (e.g. Winker et al., 2007, 2009; Mace et al., 2009; Stubenrauch et al., 2010). We recall that the analysis of a backscattered laser beam allows a vertical profiling of clouds having low optical depths (maximum about 5) with vertical resolution of about 60 m in the upper troposphere. This instrument is therefore especially efficient for the detection of cirrus clouds.

To relate ice supersaturation occurrence from AIRS to high cloud occurrence from CALIOP we determine if clouds occupy one or several AIRS pressure layers. Since ice supersaturation may occur at any location inside the pressure layers, we state that a pressure layer is occupied by a cloud when any part or proportion of the cloud is within the boundaries of the pressure layer. In that way, statistics of cirrus cloud occurrence can be computed for any pressure layer in the upper troposphere, making use of all high cloud layers, whereas passive remote sensing only provides one cloud pressure (the

Ice supersaturation from the Atmospheric InfraRed Sounder

N. Lamquin et al.

Title Page

Abstract

Introduction

Conclusions

References

Tables

Figures



Back

Close

Full Screen / Esc

Printer-friendly Version

Interactive Discussion



one of the uppermost cloud layer) when retrieved by infrared sounders (Stubenrauch et al., 1999, 2010).

Cirrus occurrence per pressure layer is then determined from two years (2007–2008) of CALIOP data. Unfortunately the lidar nadir geometry prohibits reaching very high latitudes and statistics are therefore limited to latitudes between 80° N and S. Figure 14 shows zonal means of ice supersaturation occurrence from AIRS data between 2007 and 2008 along with zonal means of cirrus occurrence, separately for the six pressure layers between 100 and 500 hPa.

The high cloud occurrence follows the ice supersaturation occurrence. This indicates the cause-to-consequence relationship between ice supersaturation and cirrus clouds: ice clouds form where ice supersaturation takes place as the latter is a prerequisite for ice cloud formation.

In Gierens et al. (2000) correlations are shown between ice supersaturation occurrence from MOZAIC and occurrence of subvisible cirrus detected from the Stratospheric Aerosol and Gas Experiment (SAGE II Wang et al., 1996). Figure 15 extends these relationships to all types of cirrus clouds with optical depth lower than about 5. The results are shown for the pressure layers below the tropopause in the tropics (0°–30° N and S separately), in the midlatitudes (30°–60° N and S separately) and in the polar regions (60°–90° N and S separately). Cirrus occurrence statistics and ice supersaturation statistics are determined for each season at a spatial resolution of 1° lat × 1° lon, only statistics with more than one hundred CALIOP measurements are used. The standard deviation in Fig. 15 represents both the seasonal variability and the spatial variability of the relationship between cirrus and ice supersaturation occurrences. In addition, the sparse sampling of CALIOP (about one orbit every 1000 km and no swath) compared to AIRS may lead to sampling noise for cirrus occurrence.

The positive correlations suggest again the cause-to-consequence relationship between ice supersaturation and cirrus clouds although the slopes of these correlations seem to decrease from about 1 in the tropics to about 0.5 in the polar regions. This could be linked to different lifetime and formation mechanisms of cirrus clouds.

Ice supersaturation from the Atmospheric InfraRed Sounder

N. Lamquin et al.

Title Page

Abstract

Introduction

Conclusions

References

Tables

Figures

◀

▶

◀

▶

Back

Close

Full Screen / Esc

Printer-friendly Version

Interactive Discussion



Although only indicative in the tropics (AIRS reliability is lower at altitudes higher than 200 hPa), the absolute difference between the layer 100–150 hPa and the other layers may be explained by higher ISS occurrence frequencies (Fig. 10) close to the tropical tropopause. The standard deviation is larger in the pressure layer 100–150 hPa than in the lower layers because ice supersaturation occurrence from AIRS is much higher during boreal winter than during boreal summer (Fig. 11) whereas cirrus cloud statistics from CALIOP do not follow such a strong variability (e.g. Nazaryan et al., 2008).

5 Comparisons with ice supersaturation occurrences from ECMWF and ECHAM

Ice supersaturation is still not represented in most global circulation models. The Integrated Forecast System (IFS) of the ECMWF (Tompkins et al., 2007) resolves supersaturation whereas the ECHAM4 climate model infers supersaturation from the cloud scheme (Burkhardt et al., 2008). Evaluations of ISS statistics with observations are required for potential improvements of ISS parametrizations (e.g. Lamquin et al., 2008; Rädcl and Shine, 2010). In the following we compare global AIRS ISS occurrence frequencies to those derived from two different models: the ECMWF forecast model and the ECHAM4 climate model. The statistics from both models are calculated using the same temperature criterion as described in Sect. 4.1.

5.1 Comparison with ECMWF

Although AIRS radiances are assimilated in the ECMWF model (McNally et al., 2006) ice supersaturation, as derived from AIRS in this study, cannot be directly assimilated. Lamquin et al. (2009) compared upper tropospheric relative humidity from the IFS and from AIRS. No comparison of ice supersaturation occurrence was possible because a method to determine ISS occurrence within the relatively large pressure layers of AIRS had not yet been developed. We are now able to perform such a comparison.

Ice supersaturation from the Atmospheric InfraRed Sounder

N. Lamquin et al.

Title Page

Abstract

Introduction

Conclusions

References

Tables

Figures

◀

▶

◀

▶

Back

Close

Full Screen / Esc

Printer-friendly Version

Interactive Discussion



Ice supersaturation from the Atmospheric InfraRed Sounder

N. Lamquin et al.

[Title Page](#)[Abstract](#)[Introduction](#)[Conclusions](#)[References](#)[Tables](#)[Figures](#)[◀](#)[▶](#)[◀](#)[▶](#)[Back](#)[Close](#)[Full Screen / Esc](#)[Printer-friendly Version](#)[Interactive Discussion](#)

For this purpose, high vertical resolution forecasts are extracted globally for the whole year 2007. They consist of 24 h-forecasts of relative humidity and temperature simulated at a spectral resolution of T799 (about 25 km at the equator) and 91 layers in the vertical (about 15 hPa). 24 h-forecasts are used rather than initial fields at 0-h lead time because of the spinup behaviour of ice supersaturation in the IFS (Lamquin et al., 2009).

We extracted data in a regular $0.5^\circ \times 0.5^\circ$ grid with vertical levels spaced by 25 hPa between 100 and 500 hPa. For the comparison the ice supersaturation occurrence frequencies in the IFS are computed using a “layer supersaturation” scheme declaring ice supersaturation present within one pressure layer (e.g. 200–250 hPa) when any of the vertical levels of this layer exhibits ice supersaturation (in this case: 200, 225 or 250 hPa). For comparison we also show zonal means obtained from ISS statistics by only considering the single level lying in the middle of the layers (here that would be 225 hPa). Consequently, the former frequencies are always higher than the latter except near the subtropics in the layers 300–400 and 400–500 hPa because of the temperature criterion (T always lower than 243 K). This criterion is applied to the bottom level for the “layer supersaturation” scheme whereas it is applied to the middle level in the other scheme, at relatively low altitudes this criterion may be fulfilled for the middle level but not for the bottom level resulting in higher occurrences of supersaturation with the middle level scheme.

Figures 16 and 17 first present climatologies of ISS occurrence frequencies from the IFS and its difference between boreal winter and summer for the year 2007. Even though the AIRS climatology covers 6 yr (only one year of data has been extracted from the IFS) Figs. 16 and 17 show a good correspondence with the geographical patterns and magnitudes seen in Figs. 10 and 11. However, for the IFS, Fig. 16 shows slightly higher frequencies in the tropics and in the regions of the storm tracks and jet streams.

For the year 2007 Fig. 18 shows the zonal means of ISS occurrence frequencies from AIRS (plain black) as well as its uncertainties (dashed black). In red, zonal means from the IFS are shown (solid line) with the dashed line indicating ISS at the middle

level of the layer. In this figure the zonal means from the IFS remain within or close to the uncertainties of our AIRS climatology. However the IFS has larger ISS occurrences in the tropics above 200 hPa, around the position of the tropopause break between 150 and 250 hPa between latitudes 40° and 60° (N and S), and in the Arctic in the pressure layer 200–250 hPa.

In the IFS, close to the tropical tropopause, ice supersaturation is taking place on a thin vertical scale around 100 hPa (see Tompkins et al., 2007). If such a model is realistic, then it is possible that AIRS agrees more with the “middle layer” ISS (here at 150 hPa) because the S-function does not capture the strong gradient of relative humidity between 100 and 150 hPa. Also, the S-function is not specifically designed for levels 100–150 and 150–200 hPa because AIRS-MOZAIC collocations are too few at such altitudes in the tropics. We also remind that we must remain cautious with the AIRS water vapour data at this altitude (Fetzer et al., 2008). The disagreements around the tropopause break and in the Arctic suggest that the ISS layer estimate (i.e. using the “layer supersaturation” scheme) more abruptly captures the transition between tropospheric and stratospheric air as supersaturation may be present at the bottom of the layer while the upper parts of it are in the stratosphere. The ECMWF ISS occurrences seem to have a stronger increase with altitude than the AIRS occurrences, which can be another side-effect of the “layer supersaturation” scheme because of the strong variability of the saturation specific humidity with temperature.

Figure 19 shows the zonal differences between boreal winter and boreal summer. The uncertainties for AIRS are determined by the sum Δ of the uncertainties from the summer and winter climatologies ($(S_{90}(\text{RH}_{iA}) - S_{110}(\text{RH}_{iA}))/2$ for each season). Again, the ECMWF ISS layer estimate lies within the uncertainties ($S_{100}(\text{RH}_{iA}) + \Delta$ and $S_{100}(\text{RH}_{iA}) - \Delta$) except near the tropical tropopause where the movement of the Inter-Tropical Convergence Zone is, however, well represented. Overall, the forecasts capture the same seasonal behaviour as the observations, especially in the polar regions where the Arctic winter brings ice supersaturation down to 400–500 hPa and where the Antarctic exhibits ISS up to 100 hPa as could be seen in Fig. 12.

Ice supersaturation from the Atmospheric InfraRed Sounder

N. Lamquin et al.

[Title Page](#)[Abstract](#)[Introduction](#)[Conclusions](#)[References](#)[Tables](#)[Figures](#)[⏪](#)[⏩](#)[◀](#)[▶](#)[Back](#)[Close](#)[Full Screen / Esc](#)[Printer-friendly Version](#)[Interactive Discussion](#)

5.2 Comparison with ECHAM

In the ECHAM4 climate model (Röckner et al., 1996) ice supersaturation frequency has been parameterized consistent with the cloud scheme (Burkhardt et al., 2008) in order to enable the simulation of the climate effect of contrail cirrus (Burkhardt et al., 2009). The parameterization uses the information on subgrid scale variability of relative humidity that is inherent in the parameterization of fractional cloud coverage and infers a fractional supersaturated area. The model has been run with a T30/L39 resolution for 5 yr and we compare the resulting climatology with observations. Vertical levels were spaced between 100 hPa and 200 hPa by 15 hPa and the spacing increased slowly to 30 hPa between 400 hPa and 500 hPa.

Due to the coarse horizontal resolution of the model we calculate the fractional supersaturated area at each level within a pressure layer. We then apply a maximum random overlap scheme (as used in the cloud scheme) in order to calculate the fractional supersaturated area for a specified layer.

Ice supersaturation occurrence is then assessed globally in the same pressure layers 100–150 hPa, 150–200 hPa, 200–250 hPa, 250–300 hPa, 300–400 hPa, 400–500 hPa at the ECHAM spatial resolution of 3.75° lat \times 3.75° lon. Figures 20 and 21 show respectively the global occurrences of ice supersaturation over the 5 yr of simulation and the difference between boreal winter and summer. We recall that results for pressure layers 100–150 and 150–200 hPa are less reliable due to the AIRS sensitivity and therefore only indicative.

Despite the low resolution of the climate model the geographical patterns and absolute values of supersaturation are quite well represented. The most obvious deficiency is that in the 150–200 hPa and the 200–250 hPa layers the climate model overestimates supersaturation frequency in the extratropics. This is due to the fact that the model's tropopause is too high in the extratropics so that those layers are too frequently part of the troposphere. The bias in tropopause height is connected with the model's lower stratospheric cold bias, a common problem in climate models (particularly at low resolution).

Ice supersaturation from the Atmospheric InfraRed Sounder

N. Lamquin et al.

Title Page

Abstract

Introduction

Conclusions

References

Tables

Figures

◀

▶

◀

▶

Back

Close

Full Screen / Esc

Printer-friendly Version

Interactive Discussion



**Ice supersaturation
from the Atmospheric
InfraRed Sounder**

N. Lamquin et al.

Title Page

Abstract

Introduction

Conclusions

References

Tables

Figures

◀

▶

◀

▶

Back

Close

Full Screen / Esc

Printer-friendly Version

Interactive Discussion



Therefore, we compare ECHAM zonal mean fractional supersaturated areas with troposphere only supersaturation frequencies from AIRS. The latter is computed using only tropospheric data (we reject data when the tropopause is lying inside the pressure layer). For comparison we also show the total (tropospheric and stratospheric) AIRS occurrences as they are computed for Fig. 18 (only computed using $S_{100}(\text{RH}_{iA})$). Additionally, ISS occurrences from AIRS have been degraded to the ECHAM spatial resolution. When ISS is computed only over tropospheric data, very few observations are taken into account for pressure layers close to the tropopause. As a consequence, pressure layers between 100 and 250 hPa can only be computed by combining all seasons as there are not enough data available separately for each season.

Figure 22 shows zonal means of AIRS (plain and dashed black as in Fig. 18 but for tropospheric data only, plain gray for tropospheric plus stratospheric data) and ECHAM ISS occurrence frequencies (plain red). Figure 23 shows the winter minus summer difference as in Fig. 19. In the tropics the ECHAM supersaturation frequencies are close to the AIRS supersaturation estimates at all levels. At lower layers ISS is mostly well reproduced except at latitudes poleward of 60° (N and S) where ISS is underestimated by ECHAM.

ECHAM4 is unable to reproduce the rise in ISS at 40° S that is connected with the southern hemispheric storm track. At the upper layers the comparison is difficult since the tropospheric only estimates of AIRS consist only of very few data. Nevertheless, ECHAM supersaturation remains mostly in between AIRS ISS and the AIRS tropospheric only ISS estimates. An exception are the midlatitudes at the 150–200 hPa layer, an area in which the IFS estimates are slightly too high as well and the AIRS data less reliable. In Fig. 23 the seasonal variations follow these observations. ECHAM shows a smaller variability of the difference between winter and summer ISS occurrences as a consequence of smaller absolute ISS occurrences.

6 Conclusions

We have presented a climatology of ice supersaturation occurrence from AIRS observations covering the period 2003–2008. The relatively coarse vertical resolution of the AIRS retrieved water vapour profiles prohibits the direct detection of shallow supersaturated layers. Therefore, we have developed a calibration method for the detection of ice supersaturation by AIRS: space and time collocations of the detection of ice supersaturation by MOZAIC with coarsely-determined relative humidity profiles from AIRS allows the determination of an a priori probability function (the “S-function”) of ice supersaturation occurrence for any relative humidity value determined by AIRS. The horizontal extent of ice supersaturation is an important feature for large-scale model parameterization, an evaluation of it is presented by use of a simple cluster analysis and its distribution can easily be fitted by a Weibull distribution.

We have used the S-function to establish a climatology of ice supersaturation occurrence over the whole upper troposphere. However, due to the lower reliability of AIRS data at high altitudes, results in pressure layers 100–150 and 150–200 hPa are only indicative. These statistics represent the probability that ice supersaturation occurs at least once within a given pressure layer. It compares relatively well to other pre-existent climatologies with high supersaturation occurrences near the tropical tropopause, in the region of the storm tracks and jet streams in the midlatitudes and close to the Arctic tropopause with a concomitant seasonal cycle. An evaluation of the climatology is presented with statistics from MOZAIC only; it shows the benefit obtained from the synergy between AIRS and MOZAIC. A correlation with cirrus cloud statistics from CALIOP shows the cause-to-consequence link between ice supersaturation and cirrus cloud formation: cirrus clouds form where ice supersaturation takes place.

Finally, we compare the AIRS climatology to model climatologies from ECMWF 24 h-forecasts and ECHAM4 between 100 and 500 hPa. Except close to the tropical tropopause and in regions with possible influence of the tropopause lying within pressure layers, the comparison with the ECMWF forecasts is good. The climatology from

Ice supersaturation from the Atmospheric InfraRed Sounder

N. Lamquin et al.

Title Page

Abstract

Introduction

Conclusions

References

Tables

Figures



Back

Close

Full Screen / Esc

Printer-friendly Version

Interactive Discussion



ECHAM4 has a lower horizontal resolution and therefore exhibits a smaller variability than AIRS and ECMWF. Nevertheless, it captures the main patterns of ISS successfully in the upper troposphere. ECHAM exhibits a smaller meridional gradient than the observations and the ECMWF model at levels below 250 hPa.

Overall, this paper presents a way of dealing with the difficulty of remotely sensing ice supersaturation and comparing statistics from various observations and models. We propose a bridge between those different means of investigation by the use of the synergy between infrared sounding and in situ measurements. Among future applications of this work a climatology of potential condensation trails from aircraft will be assessed.

Acknowledgements. This work was supported by CNRS and Ecole Polytechnique. The AIRS version 5 data were obtained through the Goddard Earth Sciences Data and Information Services (<http://daac.gsfc.nasa.gov/>) and the CALIOP data were obtained through the Atmospheric Sciences Data Center (ASDC) at NASA Langley Research Center by the ICARE Thematic Center created by CNES (<http://www-icare.univ-lille1.fr/>) and its interface ClimServ created for Institut Pierre-Simon Laplace (<http://climserv.ipsl.polytechnique.fr/>). ECMWF data have been retrieved within the framework of a special project on “Ice Supersaturation and Cirrus Clouds (SPDEISSR)”. The authors thank all the corresponding teams for assistance and public release of data products. The work contributes to COST Action ES-0604 “Water Vapour in the Climate System (WaVaCS)” and to the aforementioned SPDEISSR.



The publication of this article is financed by CNRS-INSU.

**Ice supersaturation
from the Atmospheric
InfraRed Sounder**

N. Lamquin et al.

Title Page

Abstract

Introduction

Conclusions

References

Tables

Figures

◀

▶

◀

▶

Back

Close

Full Screen / Esc

Printer-friendly Version

Interactive Discussion



Discussion Paper | Discussion Paper | Discussion Paper | Discussion Paper | Discussion Paper

References

- Burkhardt, U., Kärcher, B., Ponater, M., Gierens, K., and Gettelman, A.: Contrail cirrus supporting areas in model and observations, *Geophys. Res. Lett.*, 35, L16808, doi:10.1029/2008GL034056, 2008. 12908, 12911
- 5 Burkhardt, U. and Kärcher, B.: Process-based simulation of contrail cirrus in a global climate model, *J. Geophys. Res.*, 114, D16201, doi:10.1029/2008JD011491, 2009. 12911
- Chahine, M. T., Pagano, T. S., Aumann, H. H., Atlas, R., Barnett, C., Blaisdell, J., Chen, L., Divakarla, M., Fetzer, E. J., Goldberg, M., Gautier, C., Granger, S., Hannon, S., Irion, F. W., Kakar, R., Kalnay, E., Lambrigtsen, B. H., Lee, S.-Y., Le Marshall, J., McMillan, W. W.,
10 McMillin, L., Olsen, E. T., Revercomb, H., Rosenkranz, P., Smith, W. L., Staelin, D., Strow, L. L., Susskind, J., Tobin, D., Wolf, W., and Zhou, L.: AIRS: Improving weather forecasting and providing new data on greenhouse gases, *B. Am. Meteor. Soc.*, 87, 911–926, 2006. 12891, 12892
- Dickson, N. C., Gierens, K. M., Rogers, H. L., and Jones, R. L.: Probabilistic description of
15 ice-supersaturated layers in low resolution profiles of relative humidity, *Atmos. Chem. Phys.*, 10, 6749–6763, doi:10.5194/acp-10-6749-2010, 2010. 12899
- Divakarla, M. G., Barnett, C. D., Goldberg, M. D., McMillin, L. M., Maddy, E., Wolf, W., Zhou, L., and Liu, X.: Validation of Atmospheric Infrared Sounder temperature and water vapour retrievals with matched radiosondes measurements and forecasts, *J. Geophys. Res.*, 111, D09S15, doi:10.1029/2005JD006116, 2006.
- 20 Fetzer, E. J., Read, W. G., Waliser, D., Kahn, B. H., Tian, B., Vömel, H., Irion, F. W., Su, H., Eldering, A., de la Torre Juarez, M., Jiang, J., and Dang, V.: Comparison of upper tropospheric water vapor observations from the Microwave Limb Sounder and Atmospheric Infrared Sounder, *J. Geophys. Res.*, 113, D22110, doi:10.1029/2008JD010000, 2008. 12893, 12910
- 25 Gettelman, A., Weinstock, E. M., Fetzer, E. J., Irion, F. W., Eldering, A., Richard, E. C., Rosenlof, K. H., Thompson, T. L., Pittman, J. V., Webster, C. R., and Herman, R. L.: Validation of Aqua satellite data in the upper troposphere and lower stratosphere with in situ aircraft instruments, *Geophys. Res. Lett.*, 31, L22107, doi:10.1029/2004GL020730, 2004. 12893
- 30 Gettelman, A., Fetzer, E. J., Eldering, A., and Irion, F. W.: The global distribution of supersaturation in the upper troposphere from the Atmospheric Infrared Sounder, *J. Climate*, 19, 6089–6103, 2006a. 12891, 12897

Ice supersaturation from the Atmospheric InfraRed Sounder

N. Lamquin et al.

Title Page

Abstract

Introduction

Conclusions

References

Tables

Figures

◀

▶

◀

▶

Back

Close

Full Screen / Esc

Printer-friendly Version

Interactive Discussion



- Gettelman, A., Walden, V. P., Miloshevich, L. M., Roth, W. L., and Halter, B.: Relative humidity over Antarctica from radiosondes, satellites, and a general circulation model, *J. Geophys. Res.*, 111, D09S13, doi:10.1029/2005JD006636, 2006b.
- Gierens, K.: Are fuel additives a viable contrail mitigation option ?, *Atmos. Environ.*, 41, 4548–4552, doi:10.1016/j.atmosenv.2007.03.014, 2007.
- Gierens, K. and Brinkop, S.: A model for the horizontal exchange between ice-supersaturated regions and their surrounding area, *Theor. Appl. Climatol.*, 71, 129–140, 2002. 12903
- Gierens, K. and Spichtinger, P.: On the size distribution of ice-supersaturated regions in the upper troposphere and lowermost stratosphere, *Ann. Geophys.*, 18, 499–504, doi:10.1007/s00585-000-0499-7, 2000. 12903
- Gierens, K., Schumann, U., Helten, M., Smit, H., and Marengo, A.: A distribution law for relative humidity in the upper troposphere and lower stratosphere derived from three years of MOZAIC measurements, *Ann. Geophys.*, 17, 1218–1226, doi:10.1007/s00585-999-1218-7, 1999. 12894, 12896, 12897, 12901
- Gierens, K., Schumann, U., Helten, M., Smit, H., and Wang, P.-H.: Ice-supersaturated regions and subvisible cirrus in the northern midlatitudes upper troposphere, *J. Geophys. Res.*, 105(D18), 22743–22753, 2000. 12905, 12907
- Gierens, K., Kohlhepp, R., Spichtinger, P., and Schroedter-Homscheidt, M.: Ice supersaturation as seen from TOVS, *Atmos. Chem. Phys.*, 4, 539–547, doi:10.5194/acp-4-539-2004, 2004. 12891
- Haag, W., Kärcher, B., Ström, J., Minikin, A., Lohmann, U., Ovarlez, J., and Stohl, A.: Freezing thresholds and cirrus cloud formation mechanisms inferred from in situ measurements of relative humidity, *Atmos. Chem. Phys.*, 3, 1791–1806, doi:10.5194/acp-3-1791-2003, 2003. 12890
- Immler, F., Treffeisen, R., Engelbart, D., Krüger, K., and Schrems, O.: Cirrus, contrails, and ice supersaturated regions in high pressure systems at northern mid latitudes, *Atmos. Chem. Phys.*, 8, 1689–1699, doi:10.5194/acp-8-1689-2008, 2008. 12897
- Jensen, E. J., Smith, J. B., Pfister, L., Pittman, J. V., Weinstock, E. M., Sayres, D. S., Herman, R. L., Troy, R. F., Rosenlof, K., Thompson, T. L., Fridlind, A. M., Hudson, P. K., Cziczo, D. J., Heymsfield, A. J., Schmitt, C., and Wilson, J. C.: Ice supersaturations exceeding 100% at the cold tropical tropopause: implications for cirrus formation and dehydration, *Atmos. Chem. Phys.*, 5, 851–862, doi:10.5194/acp-5-851-2005, 2005.
- Kahn, B. H., Liang, C. K., Eldering, A., Gettelman, A., Yue, Q., and Liou, K. N.: Tropical thin

Ice supersaturation from the Atmospheric InfraRed Sounder

N. Lamquin et al.

[Title Page](#)[Abstract](#)[Introduction](#)[Conclusions](#)[References](#)[Tables](#)[Figures](#)[◀](#)[▶](#)[◀](#)[▶](#)[Back](#)[Close](#)[Full Screen / Esc](#)[Printer-friendly Version](#)[Interactive Discussion](#)

Ice supersaturation from the Atmospheric InfraRed Sounder

N. Lamquin et al.

Title Page

Abstract

Introduction

Conclusions

References

Tables

Figures

◀

▶

◀

▶

Back

Close

Full Screen / Esc

Printer-friendly Version

Interactive Discussion



cirrus and relative humidity observed by the Atmospheric Infrared Sounder, Atmos. Chem. Phys., 8, 1501–1518, doi:10.5194/acp-8-1501-2008, 2008. 12891, 12900

Kahn, B.H., Gettelman, A., Fetzer, E. J., Eldering, A. and Liang, C. K.: Cloudy and clear sky relative humidity in the upper troposphere observed by the A-train, J. Geophys. Res., 114, D00H02, doi:10.1029/2009JD011738, 2009.

Kärcher, B. and Lohmann, U.: A parametrization of cirrus cloud formation: Homogeneous freezing of supercooled aerosols, J. Geophys. Res., 107(D2), 4010, doi:10.1029/2001JD000470, 2002.

Krämer, M., Schiller, C., Afchine, A., Bauer, R., Gensch, I., Mangold, A., Schlicht, S., Spelten, N., Sitnikov, N., Borrmann, S., de Reus, M., and Spichtinger, P.: Ice supersaturations and cirrus cloud crystal numbers, Atmos. Chem. Phys., 9, 3505–3522, doi:10.5194/acp-9-3505-2009, 2009. 12891

Lamquin, N., Stubenrauch, C. J., and Pelon, J.: Upper tropospheric humidity and cirrus geometrical and optical thickness: relationships inferred from one year of collocated AIRS-CALIPSO data, J. Geophys. Res., 113, D00A08, doi:10.1029/2008JD010012, 2008. 12891, 12896, 12900, 12908

Lamquin, N., Gierens, K., Stubenrauch, C. J., and Chatterjee, R.: Evaluation of upper tropospheric humidity forecasts from ECMWF using AIRS and CALIPSO data, Atmos. Chem. Phys., 9, 1779–1793, doi:10.5194/acp-9-1779-2009, 2009. 12891, 12892, 12898, 12899, 12908, 12909

Leiterer, U., Dier, H., Nagel, D., Naebert, T., Althausen, D., Franke, K., Kats, A., and Wagner, F.: Correction method for RS80 A-Humicap humidity profiles and their validation by Lidar backscattering profiles in tropical cirrus clouds, J. Atmos. Oceanic Tech., 22, 18–29, 2005. 12898

Luo, Z., Kley, D., Johnson, R. H., and Smit, H. G. J.: Ten years of measurements of tropical upper-tropospheric water vapor by MOZAIC. Part II: assessing the ECMWF humidity analysis, J. Climate, 21, 1449–1466, 2007.

Mace, G. G., Zhang, Q., Vaughan, M., Marchand, R., Stephens, G., Trepte, C., and Winker, D.: A description of hydrometeor layer occurrence statistics derived from the first year of merged Cloudsat and CALIPSO data, J. Geophys. Res., 114, D00A26, doi:10.1029/2007JD009755, 2009. 12906

Maddy, E. S. and Barnet, C. D.: Vertical resolution estimates in Version 5 of AIRS operational retrievals, IEEE T. Geosci. Remote, 46, 2375–2384, 2008. 12891

- England, Q. J. Roy. Meteorol. Soc., 136, 1723–1732, doi:10.1002/qj.670, 2010. 12908
- Read, W.G. et al., Aura Microwave Limb Sounder upper tropospheric and lower stratospheric H₂O and relative humidity with respect to ice validation, J. Geophys. Res., 112, D24S35, doi:10.1029/2007JD008752, 2007.
- 5 Röckner, E., Arpe, K., Bengtsson, L., Christoph, M., Claussen, M., Dümenil, L., Esch, M., Giorgetta, M., Schlese, U., and Schulzweida, U.: The atmosphere general circulation model ECHAM-4: Model description and simulation of present-day climate, Max-Planck-Inst. Meteorol. Rep. 218, 90 pp., Hamburg, Germany, 1996. 12911
- Sassen, K. and Wang, Z.: Classifying clouds around the globe with CloudSat radar: 1-year of results, Geophys. Res. Lett., 45, L04805, doi:10.1029/2007GL032591, 2008.
- 10 Schumann, U.: On conditions for contrail formation from aircraft exhausts, Meteorol. Z., 5, 4–23, 1996. 12890
- Soden, B. J. and Lanzante, J. R.: An assessment of satellite and radiosonde climatologies of upper-tropospheric water vapor, J. Climate, 9, 1235–1250, 1996.
- 15 Sonntag, D.: Important new values of the physical constants of 1986, vapor pressure formulation based on the ITS-90 and psychrometer formulae, Meteorol. Z., 70, 340–344, 1990.
- Spichtinger, P. and Gierens, K. M.: Modelling of cirrus clouds – Part 1a: Model description and validation, Atmos. Chem. Phys., 9, 685–706, doi:10.5194/acp-9-685-2009, 2009a.
- Spichtinger, P. and Gierens, K. M.: Modelling of cirrus clouds – Part 1b: Structuring cirrus clouds by dynamics, Atmos. Chem. Phys., 9, 707–719, doi:10.5194/acp-9-707-2009, 2009b.
- 20 Spichtinger, P., Gierens, K., Leiterer, U. and Dier, H.: Ice supersaturation in the tropopause region over Lindenberg, Germany, Meteorol. Z., 12, 143–156, 2003a. 12891, 12898, 12899
- Spichtinger, P., Gierens, K., and Read, W.: The global distribution of ice-supersaturated regions as seen by the Microwave Limb Sounder, Q. J. Roy. Meteorol. Soc., 129, 3391–3410, 2003b.
- 25 12904
- Spichtinger, P., Gierens, K., Smit, H. G. J., Ovarlez, J., and Gayet, J.-F.: On the distribution of relative humidity in cirrus clouds, Atmos. Chem. Phys., 4, 639–647, doi:10.5194/acp-4-639-2004, 2004. 12896, 12897
- Stephens, G. L., Vane, D. G., Boain, R. J., Mace, G. G., Sassen, K., Wang, Z., Illingworth, A. J., O’Connor, E. J., Rossow, W. B., Durden, S. L., Miller, S. D., Austin, R. T., Benedetti, A., Mitrescu, C., and the Cloudsat Science Team: The CloudSat mission and the A-train, B. Am. Meteor. Soc., 83, 1771–1790, 2002.
- 30 Stubenrauch, C. J. and Schumann, U.: Impact of air traffic on cirrus coverage, Geophys. Res.

Ice supersaturation from the Atmospheric InfraRed Sounder

N. Lamquin et al.

[Title Page](#)[Abstract](#)[Introduction](#)[Conclusions](#)[References](#)[Tables](#)[Figures](#)[◀](#)[▶](#)[◀](#)[▶](#)[Back](#)[Close](#)[Full Screen / Esc](#)[Printer-friendly Version](#)[Interactive Discussion](#)

Ice supersaturation from the Atmospheric InfraRed Sounder

N. Lamquin et al.

Title Page

Abstract

Introduction

Conclusions

References

Tables

Figures

◀

▶

◀

▶

Back

Close

Full Screen / Esc

Printer-friendly Version

Interactive Discussion



Lett., 32, L14813, doi:10.1029/2005GL022707, 2005. 12891

Stubenrauch, C. J., Rossow, W. B., Scott, N. A., and Chédin, A.: Clouds as Seen by Satellite Sounders (3I) and Imagers (ISCCP): III) Combining 3I and ISCCP cloud parameters for better understanding of cloud radiative effects, *J. Climate*, 12, 3419–3442, 1999. 12907

Stubenrauch, C. J., Cros, S., Lamquin, N., Armante, R., Chédin, A., Crevoisier, C., and Scott, N. A.: Cloud properties from AIRS and evaluation with CALIPSO, *J. Geophys. Res.*, 113, D00A10, doi:10.1029/2008JD009928, 2008.

Stubenrauch, C. J., Cros, S., Guignard, A., and Lamquin, N.: A 6-year global cloud climatology from the Atmospheric InfraRed Sounder AIRS and a statistical analysis in synergy with CALIPSO and CloudSat, *Atmos. Chem. Phys.*, 10, 7197–7214, doi:10.5194/acp-10-7197-2010, 2010. 12893, 12906, 12907

Susskind, J., Barnet, C., and Blaisdell, J.: Retrieval of atmospheric and surface parameters from AIRS/AMSU/HSB data in the presence of clouds, *IEEE T. Geosci. Remote*, 41, 390–409, 2003. 12892

Susskind, J., Barnet, C., Blaisdell, J., Iredell, L., Keita, F., Kouvaris, L., Molnar, G., and Chahine, M.: Accuracy of geophysical parameters derived from AIRS/AMSU as a function of fractional cloud cover, *J. Geophys. Res.*, 111, D09S17, doi:10.1029/2005JD006272, 2006. 12892

Tobin, D. C., Revercomb, H. E., Knuteson, R. O., Lesht, B. M., Strow, L. L., Hannon, S. E., Feltz, W. F., Moy, L. A., Fetzer, E. J., and Cress, T. S.: Atmospheric radiation measurement site atmospheric state best estimates for Atmospheric Infrared Sounder temperature and water vapor retrieval validation, *J. Geophys. Res.*, 111, D09S14, doi:10.1029/2005JD006103, 2006. 12892

Tompkins, A. M., Gierens, K., and Rädel, G.: Ice supersaturation in the ECMWF Integrated Forecast System, *Q. J. Roy. Meteorol. Soc.*, 133, 53–63, 2007. 12908, 12910

Treffeisen, R., Krejci, R., Ström, J., Engvall, A. C., Herber, A., and Thomason, L.: Humidity observations in the Arctic troposphere over Ny-Ålesund, Svalbard based on 15 years of radiosonde data, *Atmos. Chem. Phys.*, 7, 2721–2732, doi:10.5194/acp-7-2721-2007, 2007. 12904

Waliser, D. E., Li, J.-L. F., Woods, C. P., Austin, R. T., Bacmeister, J., Chern, J., Del Genio, A., Jiang, J. H., Kuang, Z., Meng, H., Minnis, P., Platnick, S., Rossow, W. B., Stephens, G. L., Sun-Mack, S., Tao, W.-K., Tompkins, A. M., Vane, D. G., Walker, C., and Wu, D.: Cloud ice: A climate model challenge with signs and expectations of progress, *J. Geophys. Res.*, 114, D00A21, doi:10.1029/2008JD010015, 2009. 12891

Wang, P.-H., Minnis, P., McCormick, P., Kent, G. S., and Skeens, K. M.: A 6-year climatology of cloud occurrence frequency from Stratospheric Aerosol and Gas Experiment II observations (1985–1990), *J. Geophys. Res.*, 101(D23), 29407–29429, 1996. 12907

Winker, D. M., Pelon, J., and McCormick, M. P.: The CALIPSO mission: Spaceborne lidar for observation of aerosols and clouds, *Proc. SPIE*, 4893, 1–11, 2003. 12906

Winker, D. M., Hunt, W. H., and McGill, M. J.: Initial performance assessment of CALIOP, *Geophys. Res. Lett.*, 34, L19803, doi:10.1029/2007GL030135, 2007. 12906

Winker, D. M., Vaughan, M. A., Omar, A., Hu, Y., and Powell, K. A.: Overview of the CALIPSO mission and CALIOP data processing algorithms, *J. Atmos. Oceanic. Technol.*, 26, 2310–2323, 2009. 12906

ACPD

11, 12889–12947, 2011

Ice supersaturation from the Atmospheric InfraRed Sounder

N. Lamquin et al.

Title Page

Abstract

Introduction

Conclusions

References

Tables

Figures

◀

▶

◀

▶

Back

Close

Full Screen / Esc

Printer-friendly Version

Interactive Discussion



Ice supersaturation from the Atmospheric InfraRed Sounder

N. Lamquin et al.

Table 2. Statistics of AIRS-MOZAIC collocations (one MOZAIC single measurement per AIRS spot) in the upper troposphere separately for different AIRS cloud types. In brackets relative percentage with respect to latitude bands and total.

AIRS situation	N. Midlatitudes	Tropics	All events
Cirrus	163 070 (29.0%, 14.2% of total)	34 240 (27.3%, 3.0% of total)	290 354 (25.3%)
Lmclds	242 053 (43.1%, 21.1% of total)	17 769 (14.2%, 1.6% of total)	355 399 (31.0%)
Clear	156 750 (27.9%, 13.7% of total)	73 227 (58.5%, 6.4% of total)	500 266 (43.7%)
All situations	561 873 (100%, 49% of total)	125 236 (100%, 11% of total)	1 146 019 (100%)

[Title Page](#)
[Abstract](#)
[Introduction](#)
[Conclusions](#)
[References](#)
[Tables](#)
[Figures](#)
[Back](#)
[Close](#)
[Full Screen / Esc](#)
[Printer-friendly Version](#)
[Interactive Discussion](#)


Ice supersaturation from the Atmospheric InfraRed Sounder

N. Lamquin et al.

Table 3. Parameters a and b of the Weibull distributions fitted from the histograms of Fig. 8 and their correlation coefficient.

Case (percent above 40, 60, 80)	a	b	correlation coefficient
$S(\text{RHi}_A) > 40$, global	0.099	0.516	0.988
$S(\text{RHi}_A) > 60$, global	0.067	0.613	0.994
$S(\text{RHi}_A) > 80$, global	0.064	0.664	0.993
$S(\text{RHi}_A) > 80$, polar	0.028	0.804	0.994
$S(\text{RHi}_A) > 80$, midlatitudes	0.034	0.807	0.994
$S(\text{RHi}_A) > 80$, tropics	0.098	0.596	0.989

[Title Page](#)
[Abstract](#)
[Introduction](#)
[Conclusions](#)
[References](#)
[Tables](#)
[Figures](#)
[Back](#)
[Close](#)
[Full Screen / Esc](#)
[Printer-friendly Version](#)
[Interactive Discussion](#)

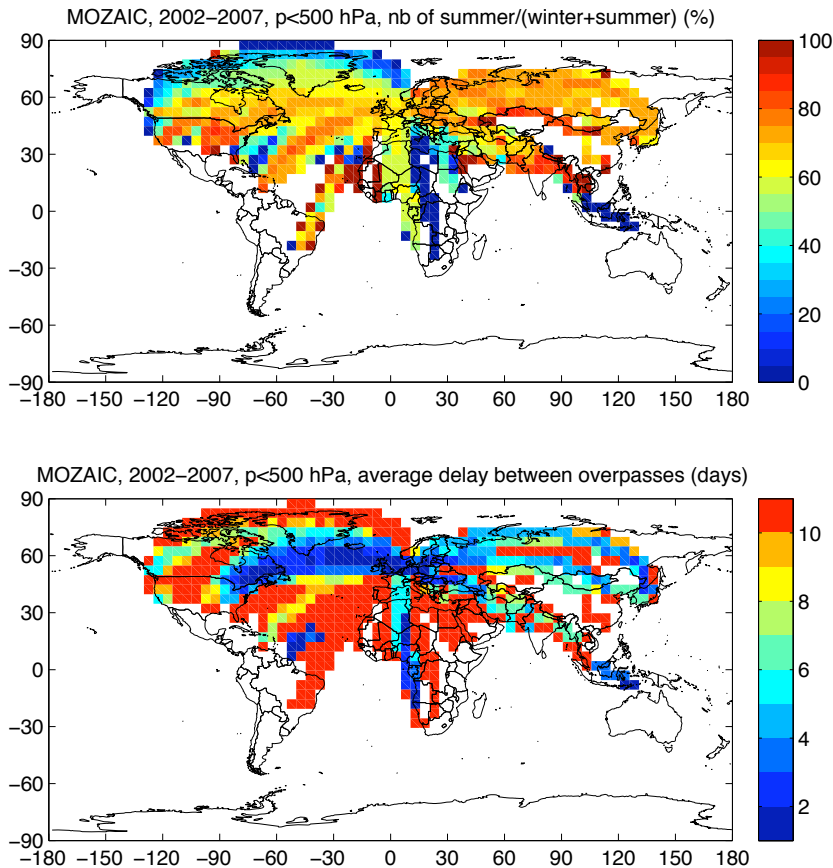



Fig. 1. Top: ratio of MOZAIC measurements taken in summer compared to the winter plus summer statistics. Bottom: average delay (in days) between two overpasses by MOZAIC flights.

Ice supersaturation from the Atmospheric InfraRed Sounder

N. Lamquin et al.

Title Page

Abstract

Introduction

Conclusions

References

Tables

Figures



Back

Close

Full Screen / Esc

Printer-friendly Version

Interactive Discussion



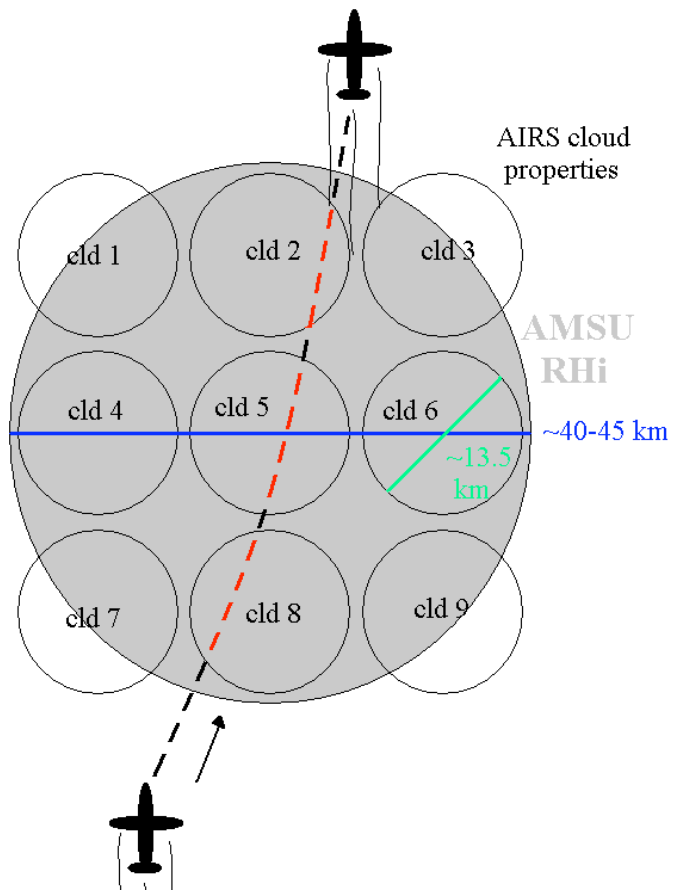


Fig. 2. Sketch of MOZAIC and AIRS collocations.

Ice supersaturation from the Atmospheric InfraRed Sounder

N. Lamquin et al.

Title Page

Abstract Introduction

Conclusions References

Tables Figures

◀ ▶

◀ ▶

Back Close

Full Screen / Esc

Printer-friendly Version

Interactive Discussion



Ice supersaturation from the Atmospheric InfraRed Sounder

N. Lamquin et al.

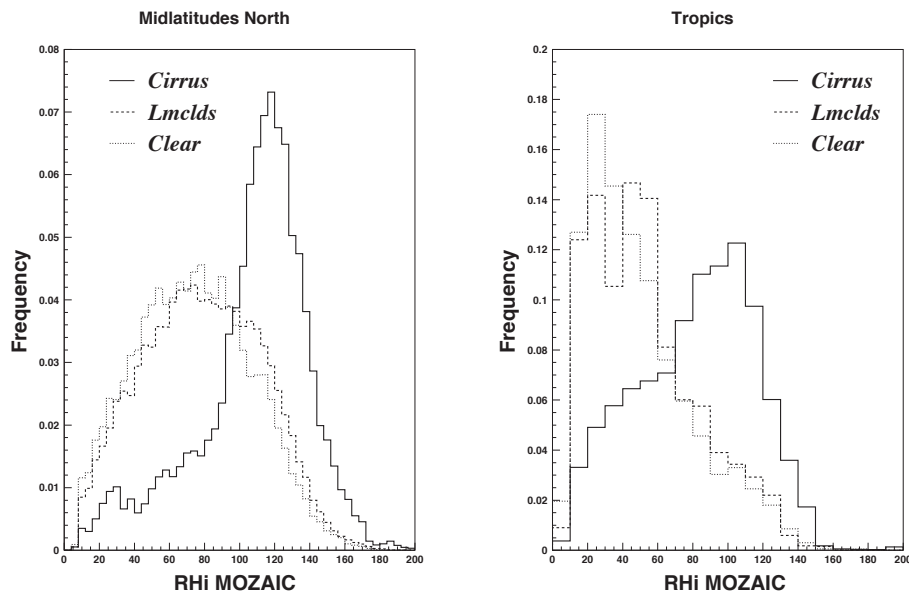


Fig. 3. Distributions of relative humidity seen by MOZAIC RH_{iM} for three classes of AIRS cloud properties in two latitude bands: northern midlatitudes (40°–60°, left) and tropics (20° N–20° S, right). For Lmclds and clear situations RH_{iM} is all measurements between 200 and 300 hPa, for cirrus situations measurements are taken at pressures close to the cloud pressure so that $|p_M - p_{cl}| < 50$ hPa. The binning for the tropics is less resolved due to the smaller sample size in the tropics.

Title Page

Abstract

Introduction

Conclusions

References

Tables

Figures

◀

▶

◀

▶

Back

Close

Full Screen / Esc

Printer-friendly Version

Interactive Discussion



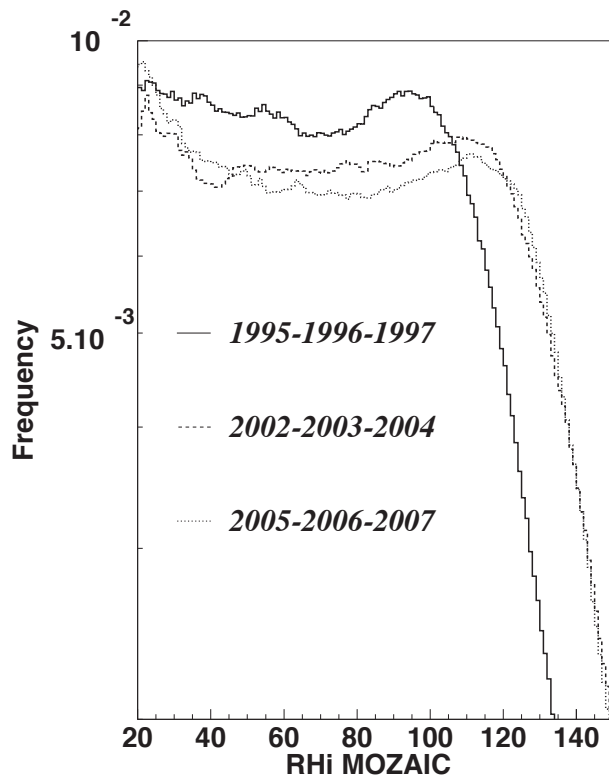


Fig. 4. Distributions of relative humidity seen by MOZAIC RH_{iM} for the years 1995-1996-1997 compared to distributions for 2002-2003-2004 and 2005-2006-2007.

Ice supersaturation from the Atmospheric InfraRed Sounder

N. Lamquin et al.

Title Page

Abstract Introduction

Conclusions References

Tables Figures

◀ ▶

◀ ▶

Back Close

Full Screen / Esc

Printer-friendly Version

Interactive Discussion



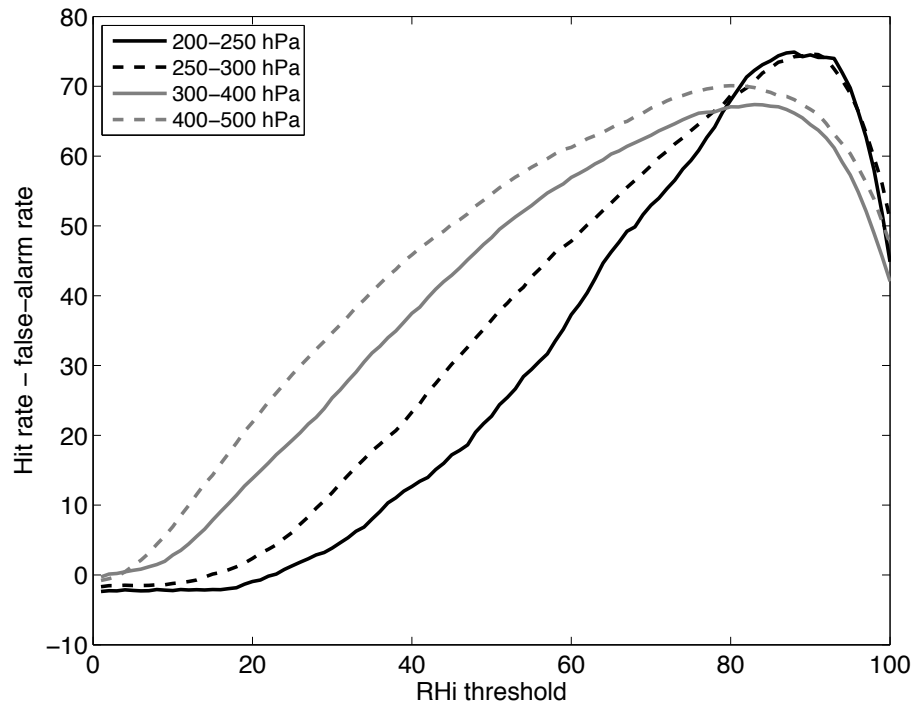


Fig. 5. Peirce skill-score simulated for four pressure layers between 200 and 500 hPa.

Ice supersaturation from the Atmospheric InfraRed Sounder

N. Lamquin et al.

Title Page

Abstract Introduction

Conclusions References

Tables Figures

◀ ▶

◀ ▶

Back Close

Full Screen / Esc

Printer-friendly Version

Interactive Discussion



Ice supersaturation from the Atmospheric InfraRed Sounder

N. Lamquin et al.

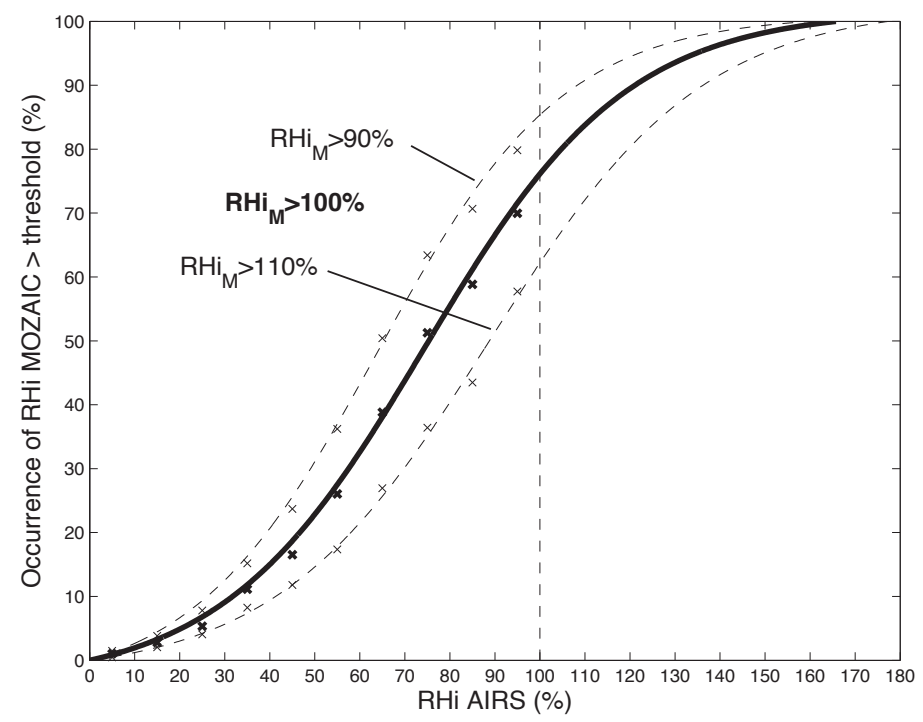


Fig. 6. Occurrence probability of ice supersaturation seen from MOZAIC as a function of AIRS relative humidity. MOZAIC supersaturation is declared when $RH_{iM} > 90\%$, $RH_{iM} > 100\%$, or $RH_{iM} > 110\%$.

Title Page

Abstract

Introduction

Conclusions

References

Tables

Figures

◀

▶

◀

▶

Back

Close

Full Screen / Esc

Printer-friendly Version

Interactive Discussion



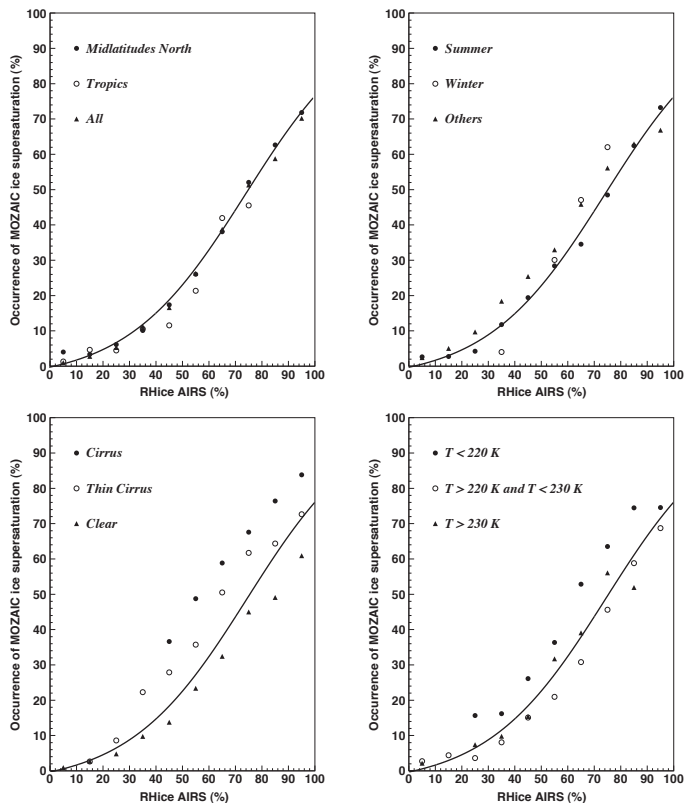


Fig. 7. Occurrence probability of ice supersaturation seen from MOZAIC as a function of AIRS relative humidity. MOZAIC supersaturation is declared when $\text{RH}_{\text{ice}} > 100\%$. Top left: sorted by regions, top right: sorted by seasons for the northern midlatitudes. Bottom left: sorted by cloud types, bottom right: sorted by temperature. In all figures the baseline S-function ($\text{RH}_{\text{ice}} > 100\%$) from Fig. 6 is reproduced in plain line.

Ice supersaturation from the Atmospheric InfraRed Sounder

N. Lamquin et al.

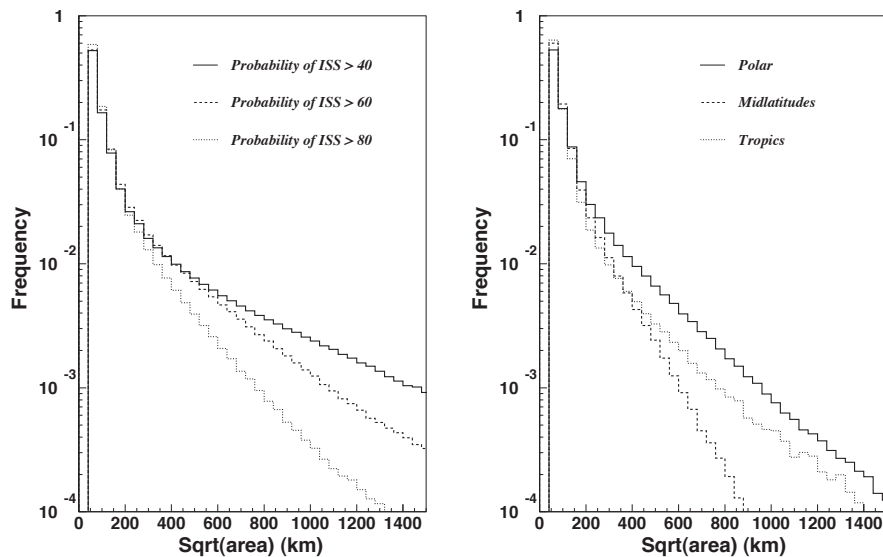


Fig. 8. Characteristic size of clusters of ice supersaturated areas from AIRS. Left: $S > 40\%$, $S > 60\%$ or $S > 80\%$, all regions combined. Right: $S > 80\%$ for polar regions (latitude higher than 70° N or S), midlatitudes (40° – 60° N and S) and tropics (20° N– 20° S).

[Title Page](#)[Abstract](#)[Introduction](#)[Conclusions](#)[References](#)[Tables](#)[Figures](#)[◀](#)[▶](#)[◀](#)[▶](#)[Back](#)[Close](#)[Full Screen / Esc](#)[Printer-friendly Version](#)[Interactive Discussion](#)

Ice supersaturation from the Atmospheric InfraRed Sounder

N. Lamquin et al.

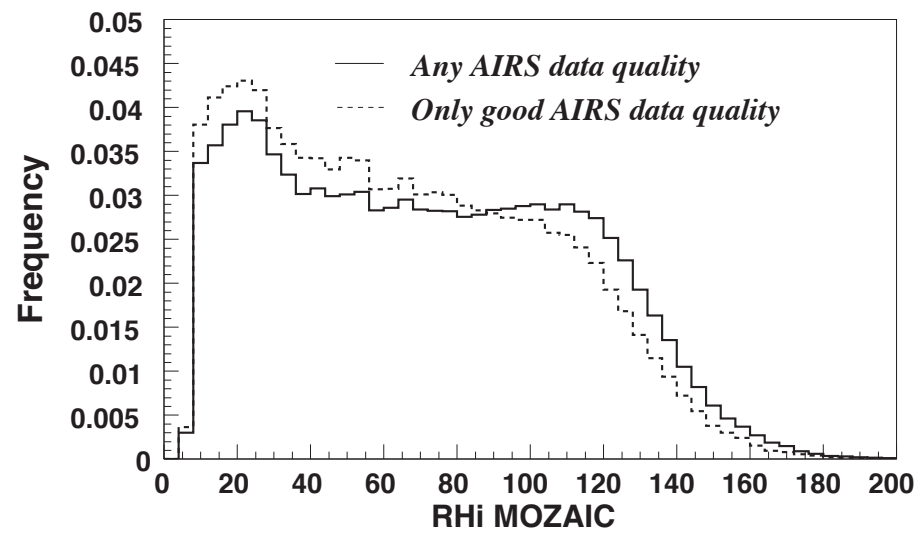


Fig. 9. Distributions of relative humidity seen from MOZAIC RHi_M in collocation with AIRS data (all qualities combined) or only with good quality AIRS data.

Title Page

Abstract Introduction

Conclusions References

Tables Figures

◀ ▶

◀ ▶

Back Close

Full Screen / Esc

Printer-friendly Version

Interactive Discussion



Ice supersaturation from the Atmospheric InfraRed Sounder

N. Lamquin et al.

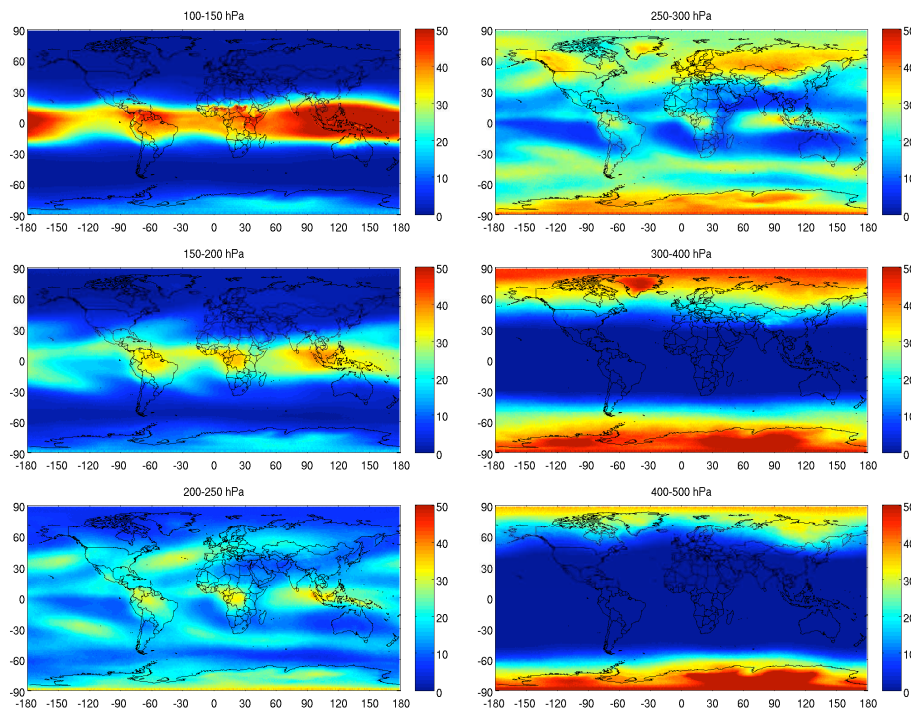


Fig. 10. Ice supersaturation occurrence frequencies (%) from AIRS in the pressure layers 100–150, 150–200, 200–250, 250–300, 300–400 and 400–500 hPa. Only good quality data used. 6-yr statistics.

[Title Page](#)[Abstract](#)[Introduction](#)[Conclusions](#)[References](#)[Tables](#)[Figures](#)[◀](#)[▶](#)[◀](#)[▶](#)[Back](#)[Close](#)[Full Screen / Esc](#)[Printer-friendly Version](#)[Interactive Discussion](#)

Ice supersaturation from the Atmospheric InfraRed Sounder

N. Lamquin et al.

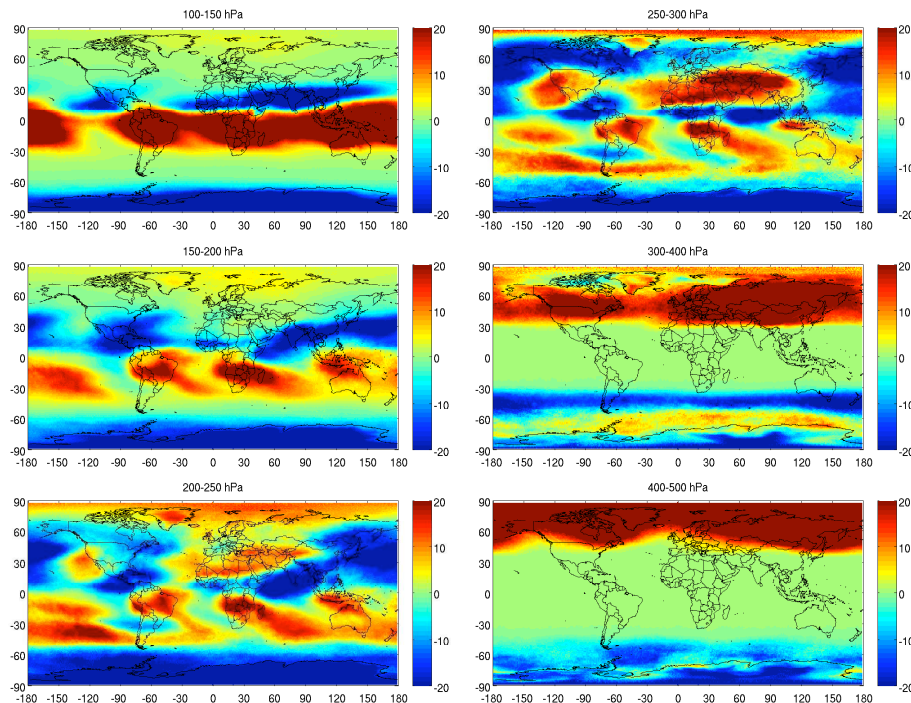


Fig. 11. Ice supersaturation occurrence frequencies (%) from AIRS in the pressure layers 100–150, 150–200, 200–250, 250–300, 300–400 and 400–500 hPa. Boreal winter – boreal summer. Only good quality data used. 6-yr statistics.

Title Page

Abstract

Introduction

Conclusions

References

Tables

Figures

◀

▶

◀

▶

Back

Close

Full Screen / Esc

Printer-friendly Version

Interactive Discussion



Ice supersaturation from the Atmospheric InfraRed Sounder

N. Lamquin et al.

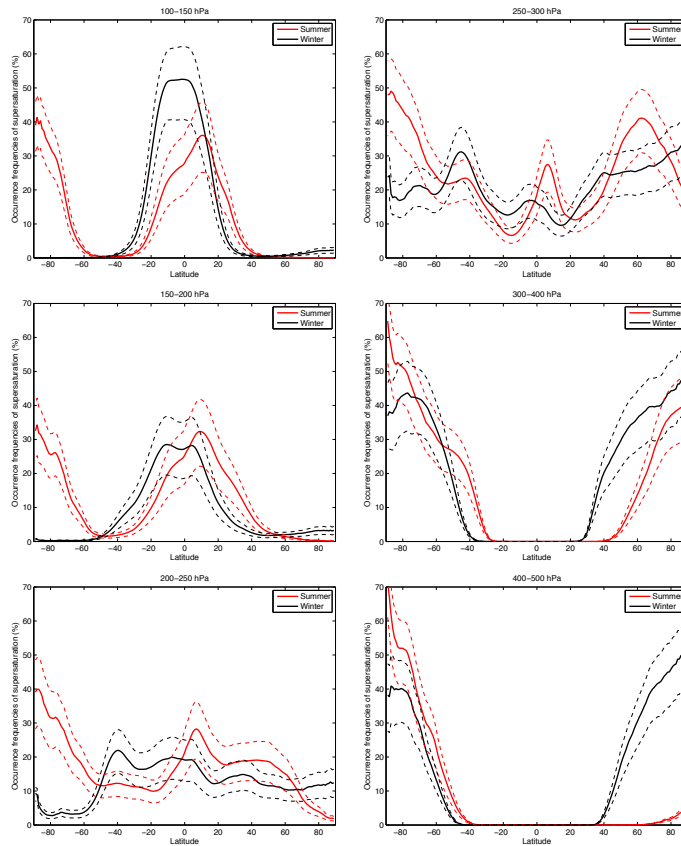


Fig. 12. Zonal means of ice supersaturation occurrence frequencies (%) from AIRS in the pressure layers 100–150, 150–200, 200–250, 250–300, 300–400 and 400–500 hPa. Plain: using $S_{100}(RH_{iA})$. Dashed: using $S_{90}(RH_{iA})$ and $S_{110}(RH_{iA})$. Winter (black lines) and summer (red lines). Only good quality data used. 6-yr statistics.

Title Page

Abstract

Introduction

Conclusions

References

Tables

Figures

◀

▶

◀

▶

Back

Close

Full Screen / Esc

Printer-friendly Version

Interactive Discussion



Ice supersaturation from the Atmospheric InfraRed Sounder

N. Lamquin et al.

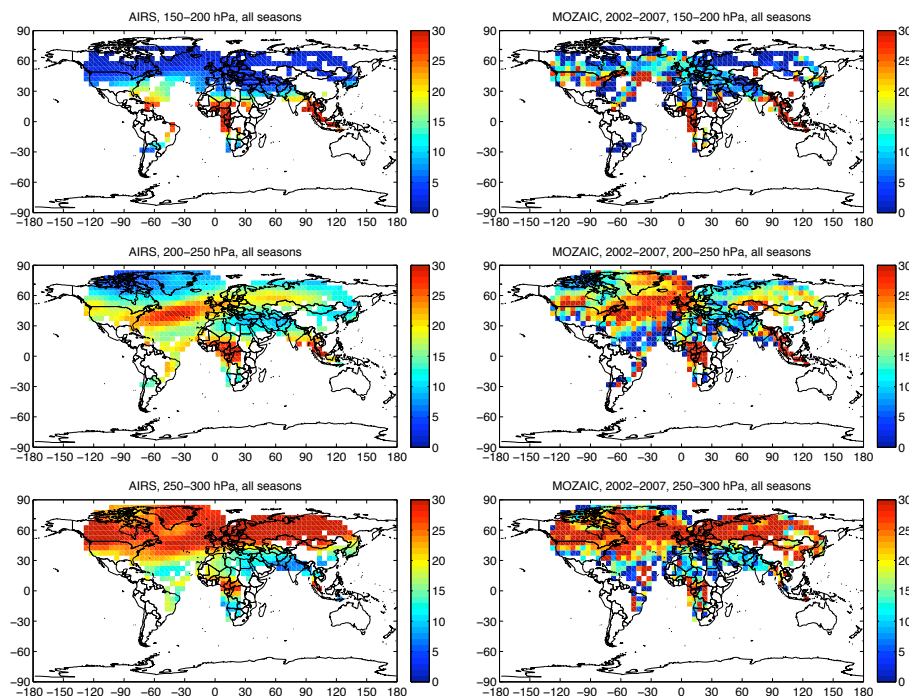


Fig. 13. Ice supersaturation occurrence frequencies (%) from AIRS (left) and MOZAIC (right) in the pressure layers 150–200, 200–250 and 250–300 hPa.

[Title Page](#)[Abstract](#)[Introduction](#)[Conclusions](#)[References](#)[Tables](#)[Figures](#)[◀](#)[▶](#)[◀](#)[▶](#)[Back](#)[Close](#)[Full Screen / Esc](#)[Printer-friendly Version](#)[Interactive Discussion](#)

Ice supersaturation from the Atmospheric InfraRed Sounder

N. Lamquin et al.

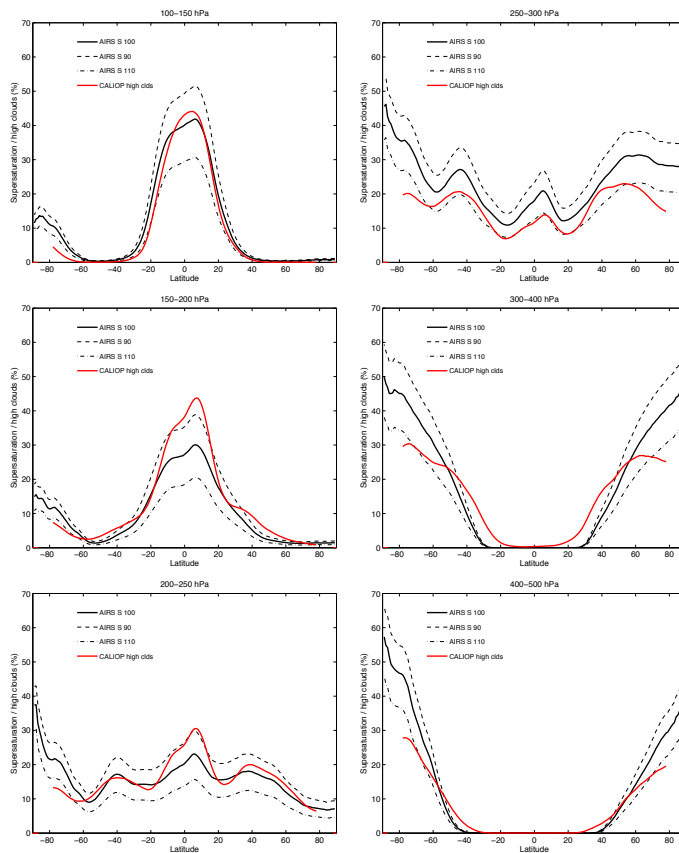


Fig. 14. Zonal means of ice supersaturation occurrence frequencies (%) from AIRS and high cloud occurrence from CALIOP for the years 2007–2008 in the pressure layers 100–150, 150–200, 200–250, 250–300, 300–400 and 400–500 hPa. Plain black: AIRS using $S_{100}(\text{RHi}_A)$. Dashed black: AIRS using $S_{90}(\text{RHi}_A)$ and $S_{110}(\text{RHi}_A)$. Plain red: CALIOP high cloud occurrence.

Title Page

Abstract Introduction

Conclusions References

Tables Figures

⏪ ⏩

◀ ▶

Back Close

Full Screen / Esc

Printer-friendly Version

Interactive Discussion



Ice supersaturation from the Atmospheric InfraRed Sounder

N. Lamquin et al.

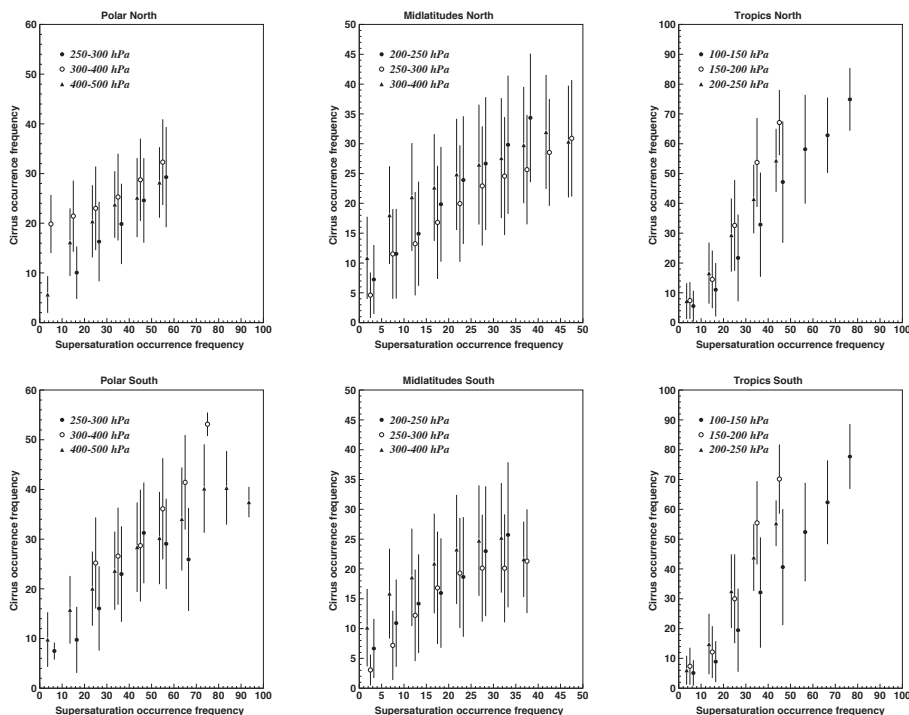


Fig. 15. Relationships between cirrus cloud occurrence frequencies (%) determined from CALIOP and ice supersaturation occurrence frequencies (%) from AIRS. Polar regions (60°–90° N and S separately), midlatitudes (30°–60° N and S separately), and tropics (0°–30° N and S separately).

Title Page

Abstract Introduction

Conclusions References

Tables Figures

◀ ▶

◀ ▶

Back Close

Full Screen / Esc

Printer-friendly Version

Interactive Discussion



Ice supersaturation from the Atmospheric InfraRed Sounder

N. Lamquin et al.

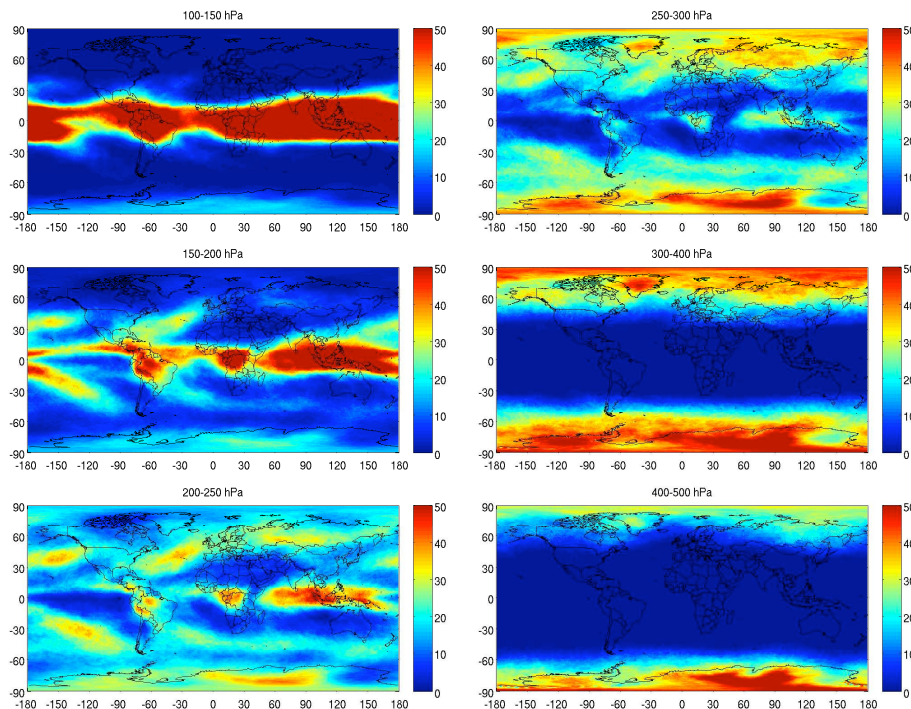


Fig. 16. Ice supersaturation occurrence frequencies (%) from ECMWF (“layer supersaturation” scheme) in the pressure layers 100–150, 150–200, 200–250, 250–300, 300–400 and 400–500 hPa. Year 2007.

[Title Page](#)[Abstract](#)[Introduction](#)[Conclusions](#)[References](#)[Tables](#)[Figures](#)[◀](#)[▶](#)[◀](#)[▶](#)[Back](#)[Close](#)[Full Screen / Esc](#)[Printer-friendly Version](#)[Interactive Discussion](#)

Ice supersaturation from the Atmospheric InfraRed Sounder

N. Lamquin et al.

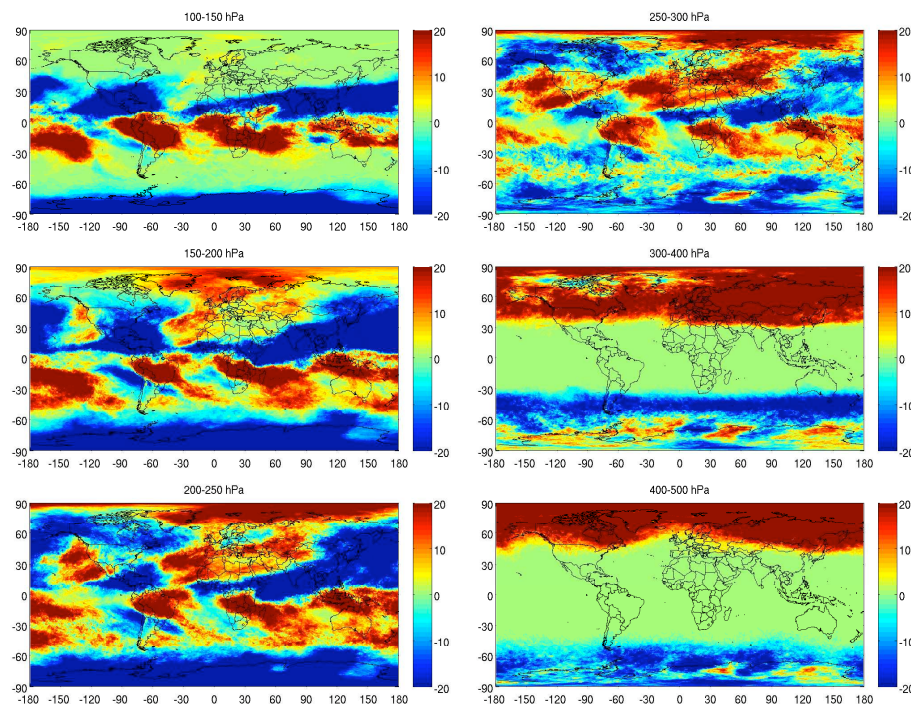


Fig. 17. Ice supersaturation occurrence frequencies (%) from ECMWF (“layer supersaturation” scheme) in the pressure layers 100–150, 150–200, 200–250, 250–300, 300–400 and 400–500 hPa. Boreal winter – boreal summer. Year 2007.

[Title Page](#)[Abstract](#)[Introduction](#)[Conclusions](#)[References](#)[Tables](#)[Figures](#)[◀](#)[▶](#)[◀](#)[▶](#)[Back](#)[Close](#)[Full Screen / Esc](#)[Printer-friendly Version](#)[Interactive Discussion](#)

Ice supersaturation
from the Atmospheric
InfraRed Sounder

N. Lamquin et al.

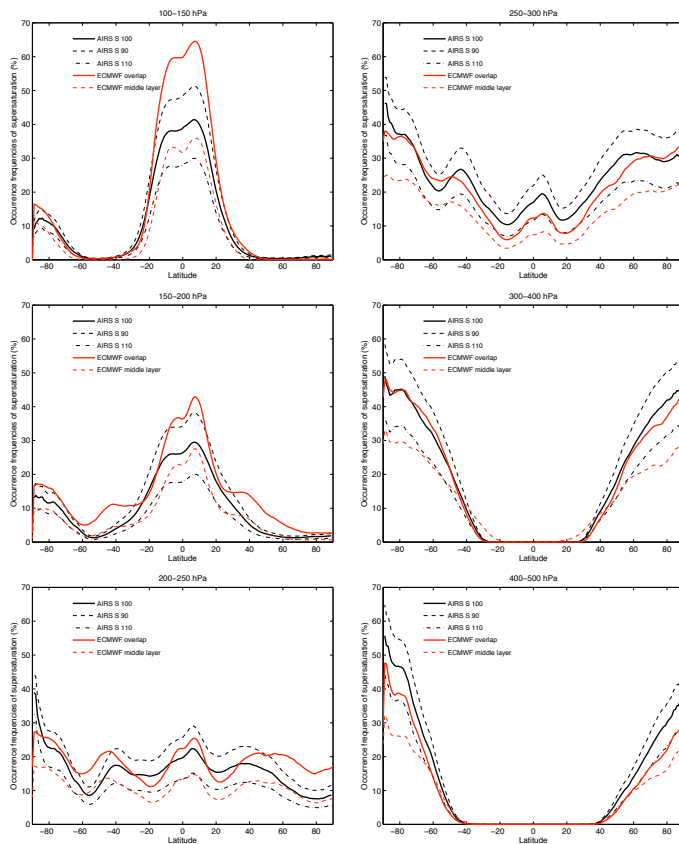


Fig. 18. Zonal means of ice supersaturation occurrence frequencies (%) from AIRS and ECMWF for the year 2007 in the pressure layers 100–150, 150–200, 200–250, 250–300, 300–400 and 400–500 hPa. Plain black: AIRS using $S_{100}(RH_{iA})$. Dashed black: AIRS using $S_{90}(RH_{iA})$ and $S_{110}(RH_{iA})$. Plain red: ECMWF using the “layer supersaturation” scheme. Dashed red: ECMWF using the “middle layer” scheme.

Title Page

Abstract

Introduction

Conclusions

References

Tables

Figures



Back

Close

Full Screen / Esc

Printer-friendly Version

Interactive Discussion



Ice supersaturation
from the Atmospheric
InfraRed Sounder

N. Lamquin et al.

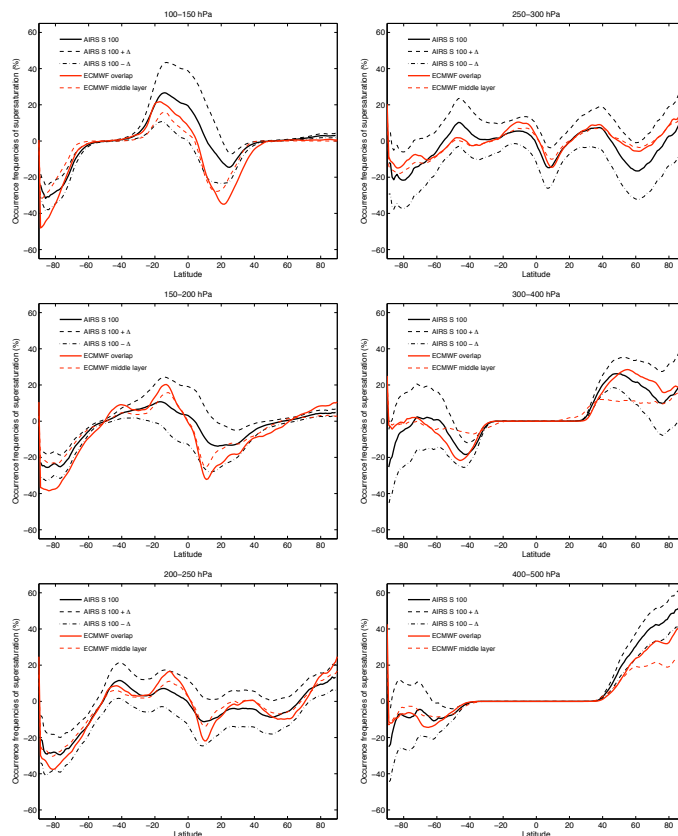


Fig. 19. Winter minus summer zonal means of ice supersaturation occurrence frequencies (%) from AIRS and ECMWF for the year 2007 in the pressure layers 100–150, 150–200, 200–250, 250–300, 300–400 and 400–500 hPa. Plain black: AIRS using $S_{100}(\text{RH}_{iA})$. Dashed black: AIRS using $S_{100}(\text{RH}_{iA}) + \Delta$ and $S_{100}(\text{RH}_{iA}) - \Delta$ where Δ is the sum of the uncertainties from $S_{90}(\text{RH}_{iA})$ and $S_{110}(\text{RH}_{iA})$. Plain red: ECMWF using the “layer supersaturation” scheme. Dashed red: ECMWF using the “middle layer” scheme.

[Title Page](#)
[Abstract](#)
[Introduction](#)
[Conclusions](#)
[References](#)
[Tables](#)
[Figures](#)
[Back](#)
[Close](#)
[Full Screen / Esc](#)
[Printer-friendly Version](#)
[Interactive Discussion](#)


Ice supersaturation from the Atmospheric InfraRed Sounder

N. Lamquin et al.

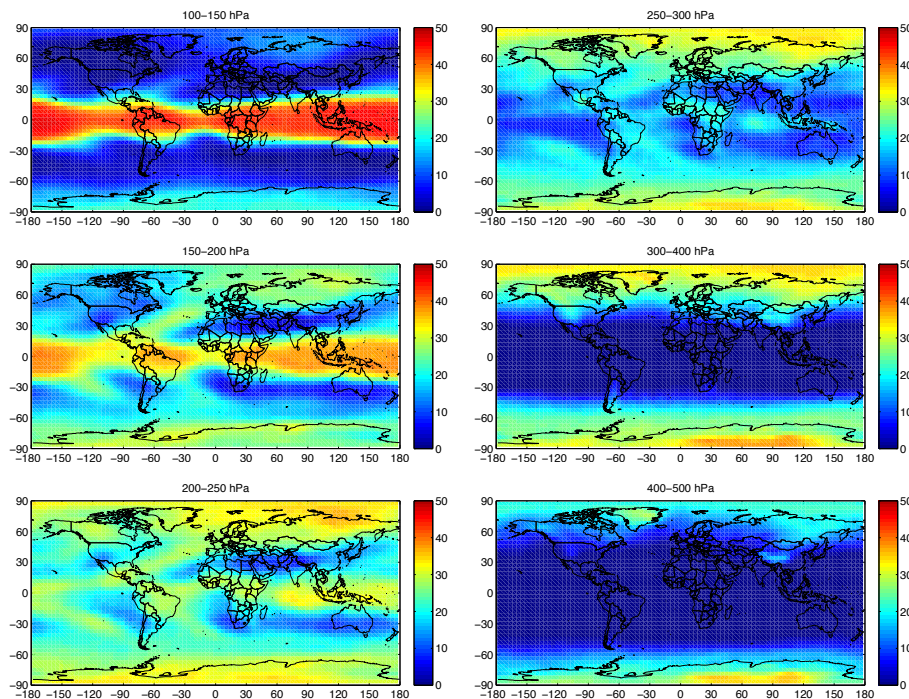


Fig. 20. Ice supersaturation occurrence frequencies (%) from ECHAM in the pressure layers 100–150, 150–200, 200–250, 250–300, 300–400 and 400–500 hPa. 5 yr of simulation.

Title Page

Abstract

Introduction

Conclusions

References

Tables

Figures

◀

▶

◀

▶

Back

Close

Full Screen / Esc

Printer-friendly Version

Interactive Discussion



Ice supersaturation from the Atmospheric InfraRed Sounder

N. Lamquin et al.

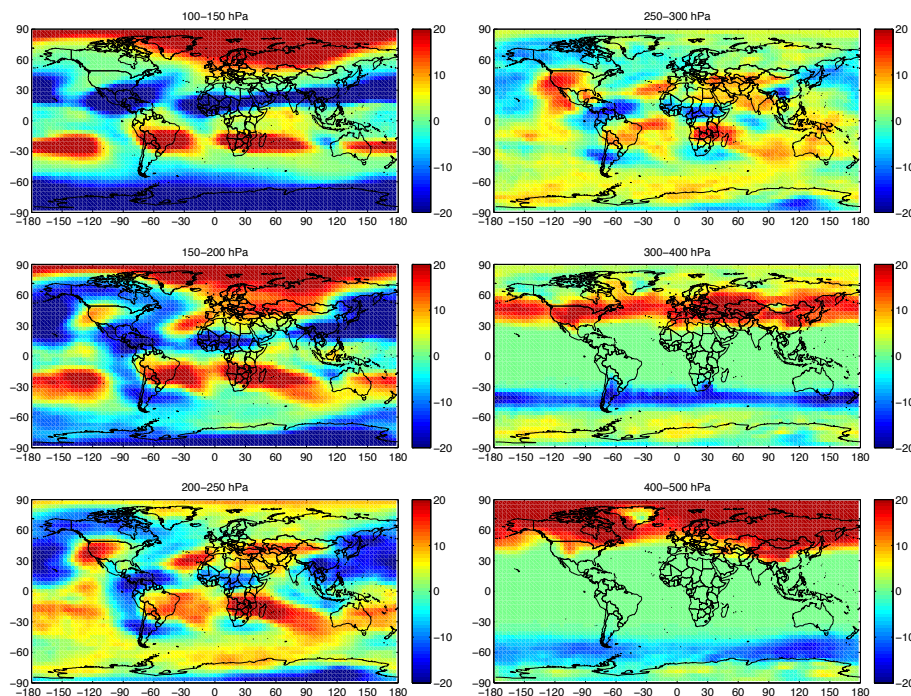


Fig. 21. Ice supersaturation occurrence frequencies (%) from ECHAM in the pressure layers 100–150, 150–200, 200–250, 250–300, 300–400 and 400–500 hPa. Boreal winter – boreal summer. 5 yr of simulation.

[Title Page](#)[Abstract](#)[Introduction](#)[Conclusions](#)[References](#)[Tables](#)[Figures](#)[◀](#)[▶](#)[◀](#)[▶](#)[Back](#)[Close](#)[Full Screen / Esc](#)[Printer-friendly Version](#)[Interactive Discussion](#)

Ice supersaturation
from the Atmospheric
InfraRed Sounder

N. Lamquin et al.

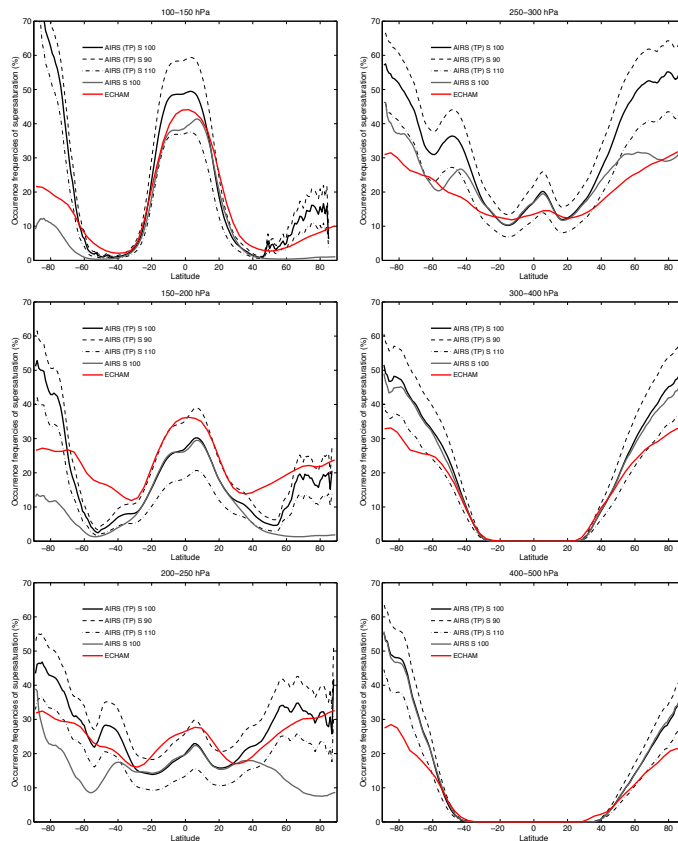


Fig. 22. Zonal means of ice supersaturation occurrence frequencies (%) from AIRS (2002–2008) and ECHAM (5 yr of simulation) in the pressure layers 100–150, 150–200, 200–250, 250–300, 300–400 and 400–500 hPa. Plain black: AIRS tropospheric data using $S_{100}(\text{RH}_{iA})$. Dashed black: AIRS tropospheric (“TP”) data using $S_{90}(\text{RH}_{iA})$ and $S_{110}(\text{RH}_{iA})$. Plain gray: AIRS global (tropospheric and stratospheric) data using $S_{100}(\text{RH}_{iA})$. Plain red: ECHAM.

Title Page

Abstract

Introduction

Conclusions

References

Tables

Figures

◀

▶

◀

▶

Back

Close

Full Screen / Esc

Printer-friendly Version

Interactive Discussion



Ice supersaturation from the Atmospheric InfraRed Sounder

N. Lamquin et al.

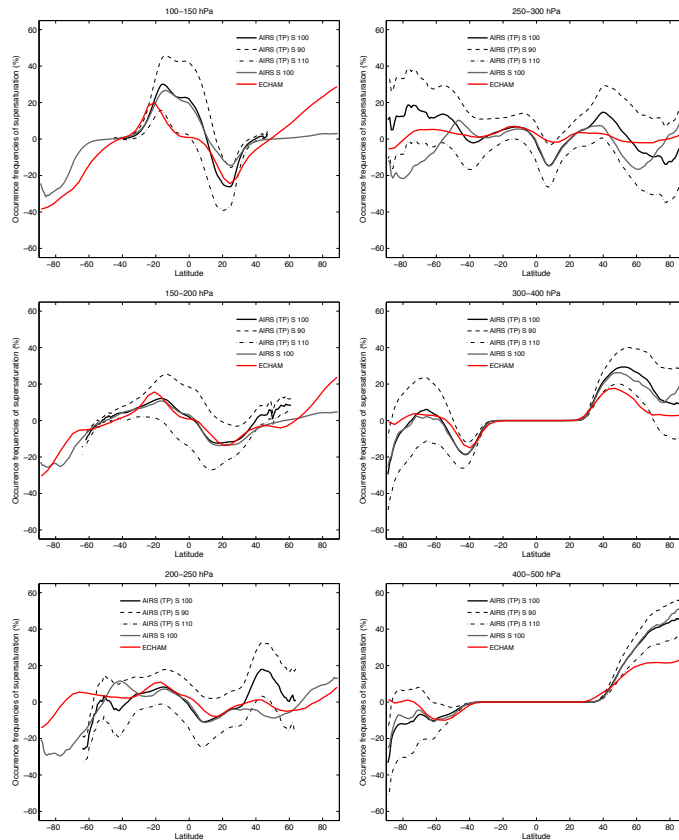


Fig. 23. Boreal winter minus summer zonal means of ice supersaturation occurrence frequencies (%) from AIRS (2002–2008) and ECHAM (5 yr of simulation) in the pressure layers 100–150, 150–200, 200–250, 250–300, 300–400 and 400–500 hPa. Plain black: AIRS tropospheric (“TP”) data using S_{100} (RH $_A$). Dashed black: AIRS tropospheric data using S_{90} (RH $_A$) and S_{110} (RH $_A$). Plain gray: AIRS global (tropospheric and stratospheric) data using S_{100} (RH $_A$). Plain red: ECHAM.

Title Page

Abstract

Introduction

Conclusions

References

Tables

Figures

◀

▶

◀

▶

Back

Close

Full Screen / Esc

Printer-friendly Version

Interactive Discussion

